Induction of CYR61 by Oncolytic HSV Infection of Glioma

A Senior Honors Thesis

Presented in Partial Fulfillment of the Requirements for Graduation
with research distinction in Biology in the Undergraduate Colleges
of The Ohio State University

By
Roopa Thakur

The Ohio State University
June 2007

Project Advisor: Dr. Balveen Kaur, College of Medicine

Acknowledgements

I would like to thank the members of the Dardinger Laboratory, Department of Neurological Surgery, for their support and guidance. I would especially like to thank Dr. Kazuhiko Kurozumi, Jayson Hardcastle, and Dr. Balveen Kaur, without whom this thesis would not have been possible.

This project was supported by grants from the National Brain Tumor Foundation, the Esther Dardinger endowment for Neuro-Oncology and Neurosciences, and the Dean's Undergraduate Research Fund – College of the Biological Sciences and Undergraduate Research Scholarship.

Table of Contents

1) Abstract **5**

2) Introduction **7**
- i) Brain Tumors: A Devastating Disease for Patients and their Families 7
- ii) Viral Oncolytic Therapy (VOLT): An Extreme Treatment for an Extreme Disease 9
- iii) HSV-1–Based Oncolytic Viruses: The Clinical Story 11
- iv) Possible limitations of VOLT in clinical trials 14
- v) Cysteine-rich Protein 61 (CYR61): A Potential Biomarker for OV Activity 17

3) Materials and Methods **22**
- i) Cells and Viruses 22
- ii) Animal Surgery 25
- iii) Immunofluorescence Staining 26
- iv) RNA Preparation 27
- v) cDNA Synthesis 28
- vi) Quantitative Real-Time PCR 28
- vii) Agarose Gel Electrophoresis 29
- viii) Harvesting Cells 29
- ix) TCA Precipitation 31
- x) SDS Preparation of In Vivo Samples 31
- xi) Protein Quantification 32
- xii) Western blots 32
- xiii) Microvessel Density Quantification 34
- xiv) Statistical Analysis 34

4) Results **35**
- i) Transcript Profiling Reveals Induction of CYR61 mRNA in Rat Glioma Tumors Treated with Oncolytic hrR3 35
- ii) Confirmation of CYR61 Induction by Quantitative Real-Time PCR (QRT-PCR) Analysis 37
- iii) Correlation between CYR61 Induction and hrR3 in Rat Brain Tumors 39
- iv) Induction of CYR61 upon hrR3 Infection of Glioma Cells *in Vitro* 39
- v) Induction of CYR61 in Glioma Cells upon Infection by Three Different HSV-1-Derived OVs *in Vitro* 40
- vi) Induction of CYR61 mRNA upon OV Infection in Human Glioma Cells *in Vitro* 42
- vii) Induction of CYR61 Protein Expression upon OV Infection of Human Glioma *in Vitro* 44
- viii) Induction of CYR61 Protein Expression upon OV Infection of Human Glioma *in Vivo* 44
- ix) Induction of Angiogenic Inducer CYR61 upon OV Treatment Leads to Increased Microvessel Density of the Residual Disease 47

5) Discussion and Conclusions **52**

6) References **54**

Abstract

Oncolytic viruses (OV) are engineered to replicate only within tumor cells, spreading within and destroying malignant gliomas without harming non-neoplastic cells. While clinical trials have confirmed its safety, the evidence for efficacy of OV therapy remains elusive. To enhance OV efficacy, a correlation linking the level of intratumoral OV over time and patient outcome/response is necessary. However, such a correlation is currently infeasible due to the lack of available biomarkers that faithfully reflect OV activity in tumors.

An initial transcript profiling of human glioma cell lines *in vitro* treated with OV revealed significant and consistent cysteine-rich 61 protein (CYR61) induction that mirrored OV presence. CYR61 is a secreted heparin-binding protein that is over-expressed in a majority of tumors, including glioma, and is a potent angiogenic factor. Thus, we hypothesized that CYR61 mRNA and protein expression will be up-regulated upon OV infection in most glioma cell lines both *in vitro* and *in vivo*, thereby indicating its use as a reliable biomarker to evaluate the efficacy of ongoing OV infection and replication in tumors.

CYR61 mRNA induction by OV infection *in vitro* was evaluated in 4 human glioma cell lines and 6 patient derived human tumor specimens using Quantitative Real Time PCR (QRT-PCR), and was confirmed in 9 out of 10 gliomas tested. We further confirmed the induction of CYR61 protein by western blot analysis of infected U343, U87, and U87ΔEGFR cells.

To verify the induction of CYR61 *in vivo*, we implanted intracerebral tumors (human U87ΔEGFR cells) in athymic nude mice and treated the tumors with OV or PBS. The harvested tumor tissue samples were analyzed for CYR61 protein expression. Finally, we checked the induction of CYR61 protein in tumors derived from human gliomas and implanted in athymic nude mice by immunofluorescent staining and confocal fluorescent microscopy.

The significant correlation between the levels of induced CYR61 and OV in tumor tissue indicates the potential usefulness of CYR61 as a biomarker for viral oncolysis in the tumor microenvironment. Our results indicate the importance of incorporating such measurements in future clinical trials using OV therapy to aid in the development of better therapeutic strategies.

Introduction

Brain Tumors: A Devastating Disease for Patients and their Families

The American Cancer Society estimates that 20,500 new cases of cancers of the brain and central nervous system (CNS) and 12,740 deaths from such malignancies will be reported in the United States in 2007. The World Health Organization (WHO) classifies brain tumors into different grades from low (Grade I) to high (Grade IV) ***(*Figure 1)**. Pilocytic astrocytomas (Grade 1) are non-infiltrative, biologically benign tumors that are usually curable upon resection [1]. The lowest grade of infiltrative astrocytoma (Grade II) is characterized by increased cellularity resulting from the percolation of neoplastic cells through the normal brain parenchyma. These tumors are most common in the cerebral hemispheres and are further typified by enlarged, hyperchromatic nuclei and irregular nuclear contours. Anaplastic astrocytomas (Grade III) represent a transition phase between Grades II and IV. These astrocytomas are characterized by the presence of nuclear pleomorphism, atypia, increased cellularity, and increased rate of proliferation. Glioblastoma multiforme (GBM), the highest grade of infiltrating astrocytoma, is described by the development of microvascular hyperplasia and/or necrosis surrounded by areas of high cellularity called pseudopalisades. Microvascular hyperplasia results from aberrant proliferation of endothelial cells, which often manifest as tufted microaggregates emerging from parent blood vessels. These aggregates are shaped like renal glomeruli and are therefore called "glomeruloid bodies" [2].

Current treatments for patients include surgical resection, radiation, and/or chemotherapy. Despite aggressive tumor resections followed by adjuvant therapy, the mean survival of patients diagnosed with GBM is about 14 months [2]. Decades of research have uncovered various molecular genetic alterations in these tumors and have led to the design of several targeted

Figure 1: Schematic of World Health Organization's (WHO) Grades of Infiltrative Astrocytoma.

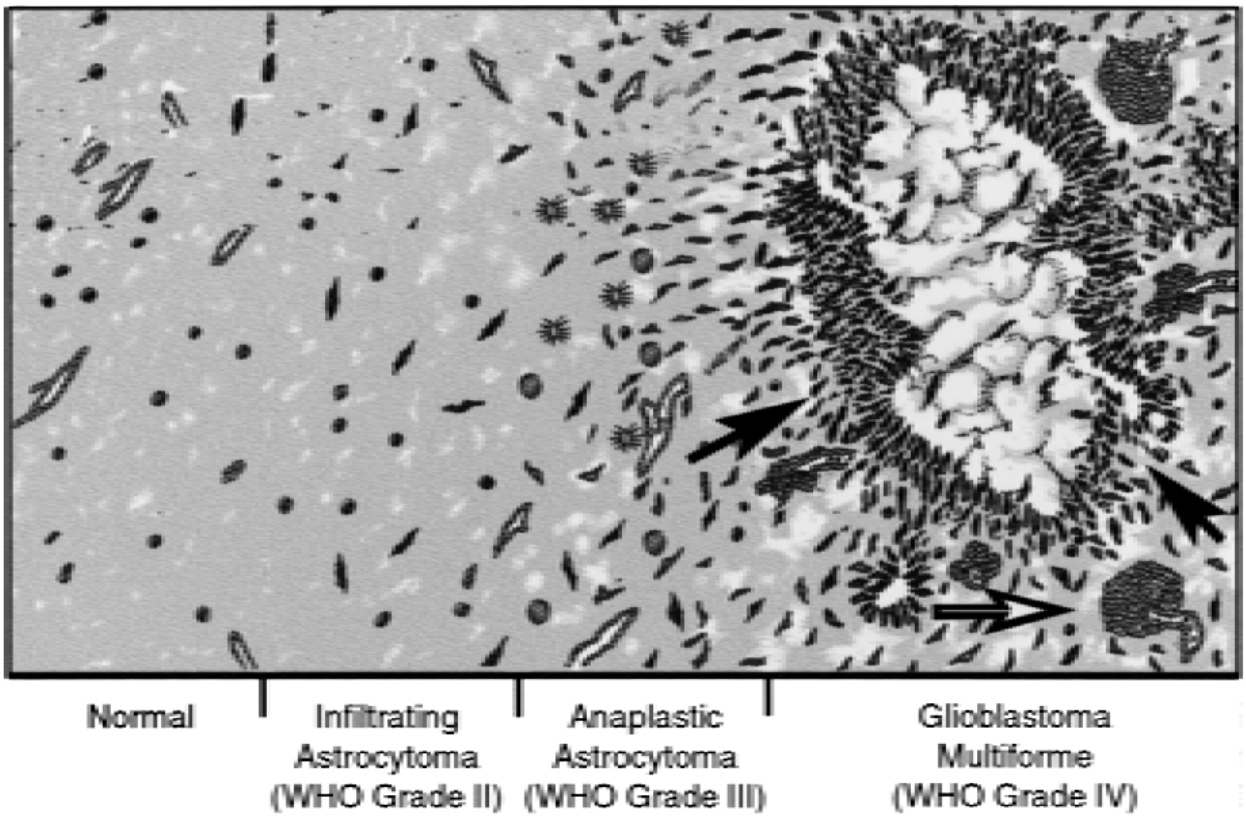

Schematic diagram of the histopathological progression of WHO infiltrative astrocytoma, grades II to IV.

Grade II brain tumors consist of individual tumor cells percolating through the CNS parenchyma. The vascular architecture and blood vessel density is similar to that of normal CNS tissue. Grade III infiltrative astrocytoma is characterized by increased cellular density, atypical morphology, and mitotic figures in anaplastic astrocytoma. They are accompanied by increasing vessel density. Glioblastoma multiforme (Grade IV malignant astrocytomas) are depicted with representative microvascular hyperplasia, glomeruloid vascularization (open arrow), and necrosis with pseudopalisading (black arrows). (Adapted from Brat, et al., *Adv Anat Pathol*, 2002 [2]).

therapeutics. However, despite intensive therapeutic interventions, these tumors are rarely curable [3]. The dismal nature of this disease underscores the need for radical treatment strategies.

Viral Oncolytic Therapy (VOLT): An Extreme Treatment for an Extreme Disease

Oncolytic virus (OV) therapy is a radical biological strategy being tested in several clinical trials in patients with malignant astrocytomas. OVs are viruses that can infect and replicate selectively within tumor cells, but not in normal non-neoplastic cells **(Figure 2)** [4,5]. Subsequent replicative cycles of the propagated virus particles enable the destruction of the tumor with minimal damage to non-cancerous tissue. Tumor-specific OVs are created via genetic manipulations of naturally occurring viruses, resulting in attenuated viruses that can replicate only in permissive cancer cells and normal cells. Some naturally occurring viruses also have a natural propensity to replicate in a tumor-specific manner and are exploited for therapy [6].

Oncolytic DNA viruses, such as herpes simplex virus- type 1 (HSV-1) and adenoviruses, are being tested in clinical trials and have revealed the relative safety of such a treatment modality [7]. A recently published report of a dose-escalating, multi-institutional trial using ONYX-015 (an attenuated adenovirus mutated for its *E1B* gene) revealed that when it was injected into glioma cavities, it was tolerated at doses as high as 10^{10} plaque forming units (p.f.u.) [8]. HSV-1–based OVs are particularly exciting because [9,10]:

1. HSV has the natural ability to infect a wide range of tissues, thereby making it applicable for treating a wide variety of tumors.

2. The inherent cytolytic nature of the virus combined with its ability to amplify to a large burst size gives it an oncolytic advantage.

3. HSV-1 has a large (152 kb) genome that is very well characterized. This provides ample opportunity for genetic manipulation to impart tumor selective

Figure 2: Oncolytic Virus (OV) Selective Infection and Destruction of Tumor Cells.

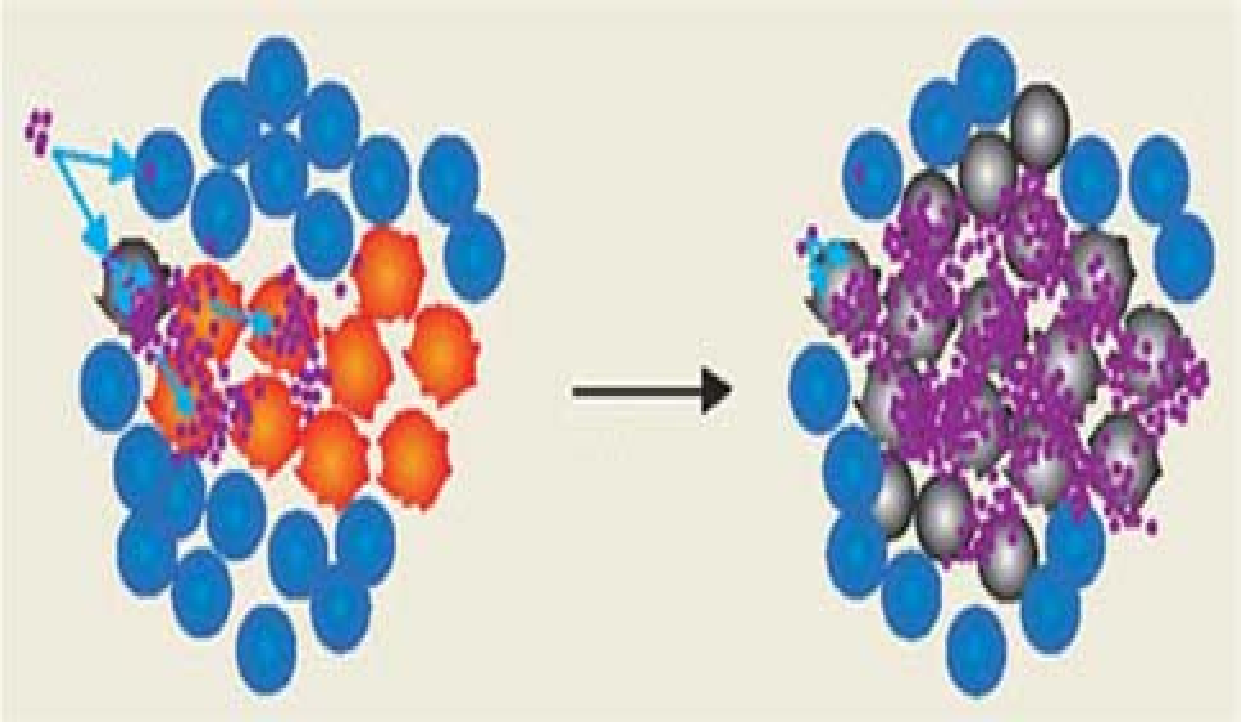

Mechanism of tumor specific destruction by OV therapy.

The principle of oncolysis by a conditionally replication-competent virus is demonstrated by tumor-specific replication of the virus. The left panel shows the initial infection of cancer cells (orange filled circles) and normal cells (blue filled circles) by infectious viral particles (purple dots). The tumor-specific replication ability of the virus results in virus replication only within the tumor cells (gray), but not in normal cells (blue). Note the destruction of tumor cells by the replicating virus, leaving adjacent normal tissue intact. (Adapted from Aguilar-Cordova E, *Nature Biotech*, 2003 [5]).

replication potential to the virus. Additionally, many of the non-essential viral genes (up to 30kb) can be replaced by therapeutic genes.

4. The inherent ability of HSV-1 virus to remain as an episome without inserting into the genome avoids the possibility of further insertional mutations in the already unstable cancer genome.

5. Finally, several anti-herpetic drugs commonly used in clinics can keep viral replication in check, if needed.

HSV-1–Based Oncolytic Viruses: The Clinical Story

The well-characterized genome of HSV-1 permits several strategies for manipulating genes to enable the tumor-selective replication of the virus. *ICP6* and *γ34.5* are two genetic loci that are frequently disrupted or otherwise altered to obtain conditionally replication-competent OVs **(Figure 3a)**. The *ICP6* gene, found at the UL39 locus, is known to code for ribonucleotide reductase (RR). *ICP6/RR* is necessary for viral replication in normal non-dividing cells because it is essential for the nucleotide synthesis required in DNA replication [11-14]. The absence of RR renders the virus unable to replicate in non-dividing cells, such as neurons, thus conferring tumor specificity to the virus. The *γ34.5* gene is encoded within repeat sequences in the viral genome (TR_L, and IR_L), and hence occurs twice in the wild-type HSV-1 genome. These regions are primarily responsible for viral neurovirulence because the gene prevents the disruption of protein synthesis that normally occurs in an infected cell's response to viral replication. Removing both copies of *γ34.5* reduces the neurovirulence of the virus by eliminating its ability to replicate in terminally differentiated cells [3].

Figure 3: HSV-1-Derived OVs Evaluated in Clinical Trials.

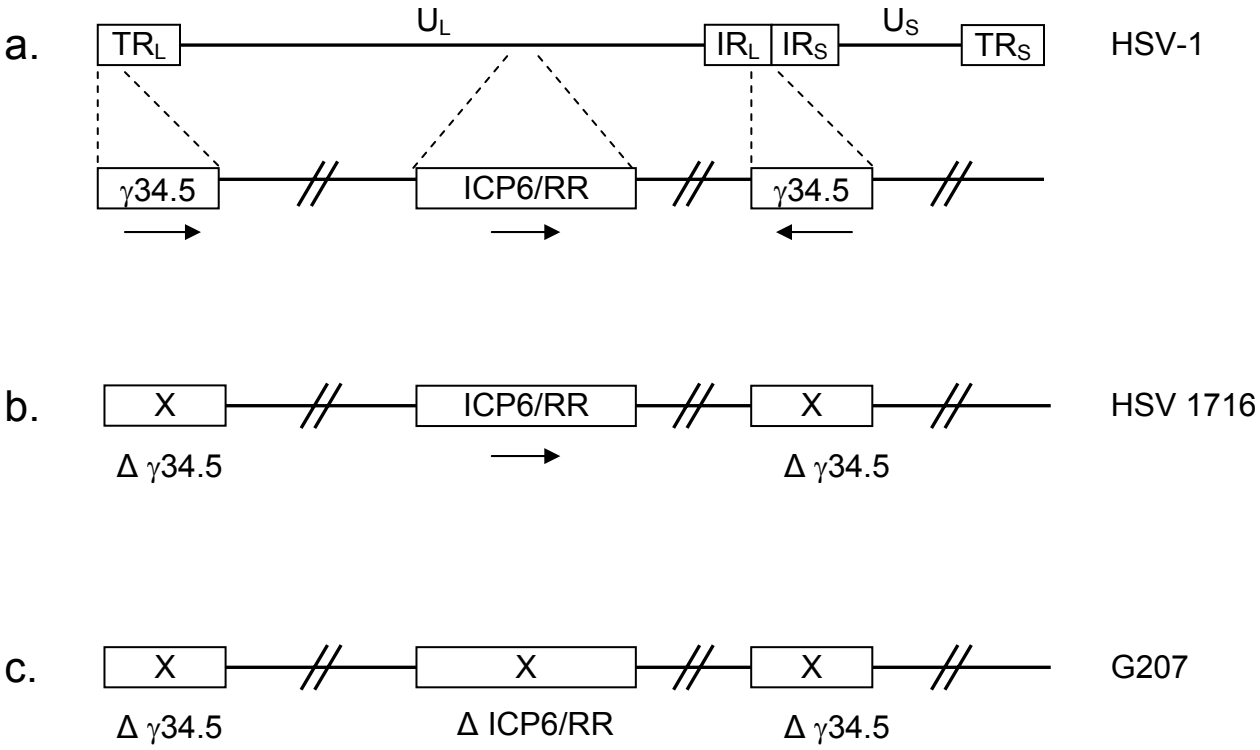

Schematic of wild type HSV-1 and two HSV derivatives tested in clinical studies: HSV 1716 and G207.

a: HSV-1 genome structure showing the U_L (Unique long sequences) and U_S (Unique small sequences). Enlargements of the U_L region depict the *γ34.5* and *ICP6* domains.

b: HSV 1716 is an HSV-1-derived OV, in which both copies of *γ34.5* have been deleted, but the *ICP6/RR* gene is retained. This mutation confers tumor specificity to the virus by rendering the virus unable to replicate in normal cells.

c: G207 is second-generation HSV-1 derivative wherein both copies of *γ34.5* have been deleted, along with the *ICP6/RR* region. These deletions result in significantly decreased neurovirulence and increased tumor specificity in OV therapy.

1716 is an oncolytic HSV from which both copies of *γ34.5* have been deleted, but it retains a functional *ICP6/RR* gene **(Figure 3b)**. In rodent models, this virus effectively destroyed rapidly dividing tumor cells without infecting surrounding brain tissue. In Glasgow, Scotland, three clinical trials have confirmed the safety of HSV 1716 as an OV. In the first trial, no adverse side effects were observed in patients suffering from recurrent malignant glioma who were treated with intratumoral inoculations of HSV 1716 at doses as high as 10^5 p.f.u. In the second trial, patients received 10^5 p.f.u. of HSV 1716 administered intratumorally. After four to nine days, resected tumors were found to have actively replicating HSV in tumor sites adjacent and distal to the site of inoculation. Again, no adverse symptoms were observed. The third study targeted residual disease by inoculating the tumor cavity following surgical resection. No signs of toxicity were observed, and three of the twelve patients survived long term (15 to 22 months) after this treatment. These clinical trials validated claims of the safety of OV therapy and provided evidence of the treatment's efficacy in a subset of patients [3].

G207 is a second-generation HSV-1 derived OV whose safety has been substantiated in various rodent models and preclinical toxicology studies. The deletion of *ICP6/RR* and both copies of *γ34.5* enable its tumor selectivity **(Figure 3c)**. Both *in vitro* and *in vivo*, infection with G207 killed glioma cells without signs of neurovirulence. Furthermore, preclinical studies in a rodent model displayed the efficacy of G207 in treating various tumor types. From these studies, a Phase 1 clinical trial using oncolytic HSV-1 was developed, in which the safety of OV therapy was confirmed [3].

Reovirus and a strain of Newcastle disease virus are other OVs undergoing clinical trials. Various strategies to enhance tumor targeting of HSV, adenoviruses, and measles virus have yielded encouraging results in preclinical studies of rodent models of cancer [15-18]. Viruses

employed as vehicles for gene transfer to cancer cells have also shown therapeutic efficacy in mice [19-22]. Despite significant advances, however, there remains a strong need for continued investigation into novel therapeutic agents for the treatment of brain cancer.

Possible limitations of VOLT in clinical trials

Although the safety of OV therapy has been confirmed in clinical trials, its efficacy remains unproven [3,4]. A thorough examination of possible reasons for the observed low efficacy is crucial to optimize benefit from this very promising treatment strategy. Inefficient viral spread, the highly attenuated nature of first-generation OVs, rapid viral clearance, technology limitations in viral production, and the lack of prognostic indicators for patient selection are thought to be some of the limitations to the success of VOLT.

The first generation of viruses that underwent clinical trials were designed to be highly attenuated due to overriding safety concerns. This attenuation may have been responsible for the decreased efficacy of infection of cancerous cells that was observed in the trials. The restricted expression of viral receptors on most cancer cells may also contribute to the decreased ability of virus to infect cancer cells. Both of these hindrances require the engineering of a second generation of genetically modified OVs that are more potent, but maintain current levels of safety [4,11].

Brain tumors, like other solid tumors, are composed of neoplastic cells as well as normal stromal cells embedded in an extracellular matrix (ECM) composed of secreted proteins, proteases, and growth factors. The complex ECM of a solid tumor plays a very significant role in limiting the spread of large therapeutic molecules, such as a virus, to distal regions of the tumor. Modulation of the ECM has been shown to enhance viral spread and thereby increase

OV efficacy [23,24]. Thus, efforts to understand and modify the tumor microenvironment are essential to enhance viral efficacy [4].

Limitations in current technology may also hinder therapeutic efficacy because the viruses may not be produced at high enough titers to be effective. However, this idea contradicts the underlying principle of virus therapy, wherein a single viral particle should be able to infect, replicate, and destroy the entire mass of tumor cells. Though this theory holds true *in vitro*, after initial OV inoculation *in vivo,* viral titers in tumors have been observed to decline [4,25].

The decrease in viral titers *in vivo* may result from the rapid neutralization, degradation, and clearance of viral particles that result from the host's immune response [4]. Upon infection with virus, the host's innate immune response is activated, which then stimulates viral clearance from cells and thereby limits further OV therapy [26-28]. This theory is bolstered by recent observations that transient immune suppression using cyclophosphamide (CPA) enhanced the therapeutic efficacy of the administered OV by reducing viral clearance by the host's innate immune responses, thus allowing better oncolysis of tumor tissue **(Figure 4)** [28,29]. On the other hand, OV-mediated lysis of cancer cells is also thought to be responsible for activating a systemic adaptive anti-tumor immune response [30-32]. The significance of these paradoxical effects of the host immune responses on the OV therapy is not very clear.

Despite anecdotal reports of patients' with brain tumors responding to OV therapy, its efficacy has not been proven. Due to limitations in current technology it is not possible to correlate individual patient responses with effective OV infection, replication, and propagation in tumors [6]. OV efficacy is currently measured by assessing the presence of viral particles and/or lysed tumor cells in patient serum. However, neither of these markers accurately represents OV activity and may actually reflect either viral clearance or tumor destruction by anti-tumor

Figure 4: Cyclophosphamide (CPA) Pretreatment Suppresses Host Immune Responses Responsible for Rapid Viral Clearance.

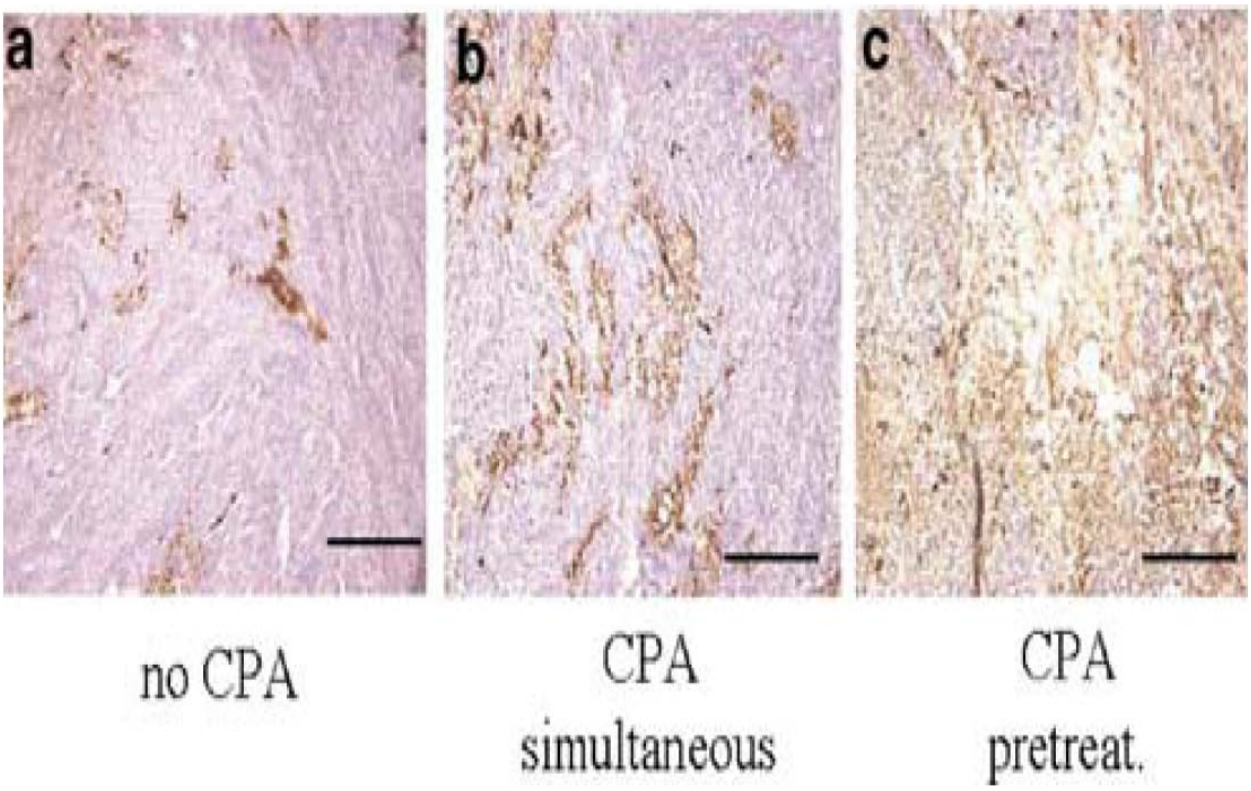

CPA pretreatment suppresses host immune responses, thereby inhibiting rapid viral clearance and allowing increased viral replication.

Immunohistochemistry for HSV capsid protein on brain sections derived from tumor bearing rats with tumors treated with CPA and/or HSV-1-derived OV, as indicated. Panel a depicts a representative tumor section from animals treated with oncolytic virus hrR3 alone. In panel b, a typical section is shown from animals treated with hrR3 and CPA on the same day. Panel c depicts a representative section of tumors harvested from animals that were pretreated with CPA 2 days prior to hrR3 treatment. In each panel, the brown precipitates are indicative of HSV capsid antigen expression. Note the significant increase in HSV presence in tumors from animals pretreated with CPA. This increase indicates CPA inhibition of viral clearance, which allows increased viral replication and infection. The scale bar represents 100 μm. (Adapted from Wakimoto, et al. *Gene Ther*, 2004 [29])

immune responses. This underscores the need for development of a biomarker that (1) can accurately reflect OV activity in patient tumors, and (2) can be used to correlate its presence with patient response in clinical trials.

We have been elucidating changes in tumor microenvironment in response to OV therapy and have identified the induction of cysteine-rich protein 61 (CYR61) in glioma cells upon infection with oncolytic HSV.

Cysteine-rich Protein 61 (CYR61): A Potential Biomarker for OV Activity

CYR61 is a ≈ 40kDa secreted heparin-binding protein encoded by a growth factor-inducible immediate-early gene. CYR61 is a member of the Cysteine-rich 61/Connective tissue growth factor/Nephroblastoma overexpressed (CCN) family of growth factors [1,33-35]. The protein sequence predicts it to have several conserved domains (SMART domain analysis: http://smart.embl-heidelberg.de/smart/show_motifs.pl, 5/4/2007): IGFBP-domain, von Willebrand factor-domain, thrombospondin-domain, and a C-terminal cysteine knot **(Figure 5)**.

These conserved domains, when compared to proteins with homologous amino acid sequences, reveal some potential functions of the CYR61 protein. For example, insulin growth factor-binding proteins (IGFBP) prolong the half-life of insulin-like growth factors (IGF) and seem to alter the interactions between IGFs and their cell surface receptors. In cell culture, IGFBPs have been observed to either inhibit or stimulate the growth-promoting effects of IGFs.

The von Willebrand factor (VWF) type C repeat is found in various plasma proteins: complement factors B, C2, CR3 and CR4; the integrins (I-domains); collagen types VI, VII, XII and XIV; and other extracellular proteins. Most VWF-containing proteins are extracellular and involved in multiprotein complexes. This domain is often found in multidomain/multifunctional proteins involved in homeostasis. Proteins containing VWF domains also participate in cell

Figure 5: Predicted Domain Structure of Cyr61.

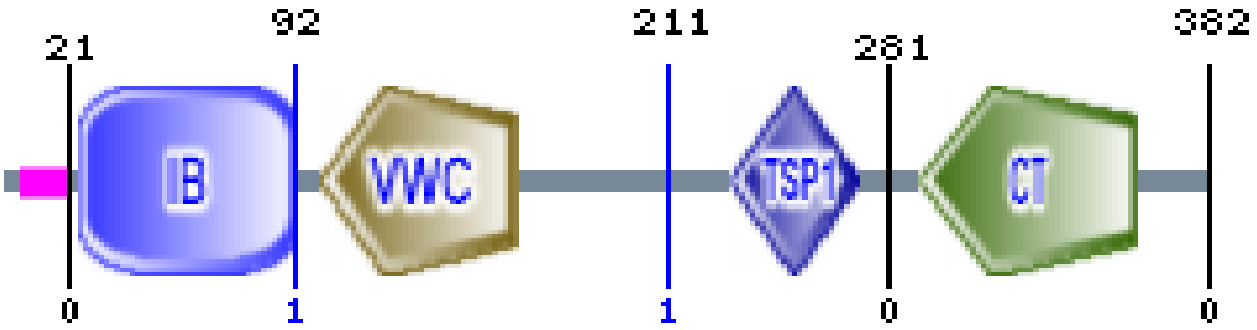

Prediction of CYR61's domain structure by comparison to homologous domains.

IB: Insulin growth factor-binding protein (IGFBP) domain is found in IGFBP. The IGFBP are characterized by high affinity binding to insulin-like growth factors (IGF). Position in CYR61: amino acids 24 to 93; E-value = 1.16e-24.

VWC: von Willebrand factor type C domain is common in extracellular proteins that are involved in multi-protein complexes. Position in CYR61: amino acids 100 to 163; E-value = 3.28e-23.

TSP-1: Thrombospondin type 1 repeats bind and activate TGF-beta. Position in CYR61: amino acids 231 to 273; E-value = 5.43e-06.

CT: C-terminal cystine knot-like domain (CTCK) is a non-globular domain that is predicted to form homo- and heterodimers. Position in CYR61: amino acids 291 to 360; E-value = 6.88e-23.

(Adapted from SMART domain analysis: http://smart.embl-heidelberg.de/smart/show_motifs.pl, 5/4/2007)

adhesion, migration, homing, pattern formation, signal transduction, and interactions with ligands.

The thrombospondin type 1 (TSP-1) repeat has been identified in thrombospondin protein; complement pathway proteins (properdin, C6, C7, C8A, C8B, C9); and extracellular matrix proteins (mindin, F-spondin, SCO-spondin, circumsporozoite surface protein 2, and TRAP proteins of Plasmodium). The TSP-1 domain is associated with cell-to-cell interaction, apoptosis, and inhibition of angiogenesis.

Despite a lack of sequence homology, the C-terminal cystine knot-like (CTCK) region is characterized by a distinctive arrangement of six cysteines that form a "cystine-knot" and is shared by structurally related growth factors from four different superfamilies. As a result of their distinctive shape, these proteins are active as either homo- or heterodimers (SMART domain analysis: http://smart.embl-heidelberg.de/smart/show _motifs.pl).

CYR61 is expressed in a variety of cells, including those of the vasculature and the muscle, bone and nervous systems. It is also expressed highly during development and in pathological states in adulthood [36]. Because of its ability to bind to heparin sulfate proteoglycans, CYR61 is associated with the ECM and cell surface, and thus is usually not detected in the culture medium [34,37]. Consistent with its localization in the ECM, CYR61 functions as a cellular adhesion molecule that is key in communicating changes in the cellular environment to the cell [37,38]. It is known to promote cell proliferation, adhesion, migration, and differentiation [1,33]. CYR61 is rapidly induced in response to mechanical stress or injury and has been implicated as a major player in the regulation of angiogenesis, matrix remodeling, and wound healing [34,39-42].

Although CYR61 can promote cellular proliferation in a variety of tissues, it is also known to activate apoptotic pathways in other cell types. For example, studies have indicated its function in neural death via the JNK signal pathway as well as in the binding of integrins [33,43-45]. In fibroblasts, CYR61 mediates cell adhesion by acting as a ligand of integrin $\alpha_V\beta_3$, and its transcription in these cells is rapidly activated by serum or purified platelet-derived growth factor without requiring *de novo* protein synthesis [34,37]. CYR61 upregulation in response to Coxsackievirus infection of human fibroblasts has also been found to enhance virus-mediated cell death [33].

While CYR61 expression can induce apoptosis in fibroblasts, its expression in some tumors has been correlated with a highly aggressive phenotype and functions as a poor prognostic indicator. Its overexpression in a variety of malignancies – including those of the breast, prostate, and brain – correlates with a poor prognosis [1,33,46-49]. CYR61 has also been associated with accelerated tumor growth and vascularization in athymic nude mice *in vivo* [35]. Overexpression of CYR61 in glioma cells has been observed to accelerate cellular growth and adhesion *in vitro* [34].

Preliminary studies in Dr. Kaur's laboratory have revealed that CYR61 mRNA is induced in glioma cells of experimental rat brain tumors upon infection with oncolytic HSV-1. Based on these results, we hypothesize that CYR61 mRNA transcription is induced following OV infection, both *in vitro* and *in vivo*, in a variety of cancerous glioma cell lines. Furthermore, we hope to validate an increase in CYR61 protein expression in glioma cells after OV infection *in vitro* as well as *in vivo*. These increases in CYR61 expression will confirm protein induction following OV infection and thereby signify that CYR61 overexpression in OV-treated tumors can be used as an indicator of virus survival and propagation. This study may ultimately lead to

the development of CYR61 as a biomarker for evaluating the tumor oncolysis by HSV-1–derived OV.

Materials and Methods

Cells and Viruses

Human U343, U87, U87ΔEGFR, and LN229 glioma cell lines were maintained in Dulbecco's modified minimal essential medium (DMEM) supplemented with 2% fetal Bovine serum (FBS), 100 U/ml penicillin, and 100 μg/ml streptomycin. Rat glioma D74/HveC cells were derived from rat glioma D74 and were stably transfected with human HveC receptor to facilitate HSV infection [29]. These cells were maintained in Dulbecco's modified minimal essential medium (DMEM) supplemented with 2% fetal Bovine serum (FBS), 100 U/ml penicillin, and 100 μg/ml streptomycin and 3.7 μg/ml blasticidin. U87ΔEGFR cells express a truncated, constitutively active, mutant form of epidermal growth factor receptor (EGFR) and were maintained in DMEM supplemented with 2% fetal Bovine serum (FBS), 100 U/ml penicillin, and 100 μg/ml streptomycin and 200 μg/ml G418 [50].

Human patient tumor derived primary tumor cells were obtained from Dr. Akihiro Otsuki (Department of Neurological surgery, The Ohio State University). These cells were grown as a monolayer in DMEM supplemented with 2% serum. See **Table 1** for details on the sources of these primary tumor cell lines.

We have been using HSV-1-derived oncolytic viruses: HSVQ, hrR3, rQNestin34.5, and rQ1-α-Fluc. The genetic structure of wild type HSV-1 and the various OVs used in this study are shown in **Figure 6**. hrR3 is a mutant of HSV-1-derived OV that lacks a functional *ICP6* gene, which codes for ribonucleotide reductase (RR), at the UL39 locus. RR is essential for nucleotide synthesis required for DNA replication [11-14]. The absence of RR is compensated in cycling cancerous cells but not in normal non-dividing cells. In hrR3, RR is disrupted by the insertion of an E. coli *LacZ* gene, resulting in the ability of the virus to replicate specifically in

Table 1: Sources of Patient-Derived Primary Tumor Cell Lines.

Cell Line Name	Diagnosis	Sex	Age	Location	Primary/ Recurrent	Prior therapy
OG02	GBM	M	47	Left Frontal lobe	Recurrent GBM	Chemotherapy and/or radiation.
OG06	Glioma	F	51	Left temporal parietal lobes	Primary	NA
OG08	GBM	M	58	Right temporal	Primary	NA
OG09	GBM	M	69	Left temporal	Primary	NA
# 8.0	GBM	M	59	Left Occipital Lobe	Primary	NA
# 9.0	glioma	F	64	Right temporal	Primary	NA

Sources of primary tumor cell culture.

Human patient tumor derived primary tumor cells were obtained courtesy of Dr. Akihiro Otsuki (Department of Neurological surgery, The Ohio State University). In culture, the cells were grown as a monolayer in DMEM supplemented with 2% fetal bovine serum (FBS). Abbreviations: GMB - Glioblastoma multiforme; M - Male; F - Female; NA - Not applicable.

Figure 6: Schematics of HSV-1 Derivatives used in OV Treatment.

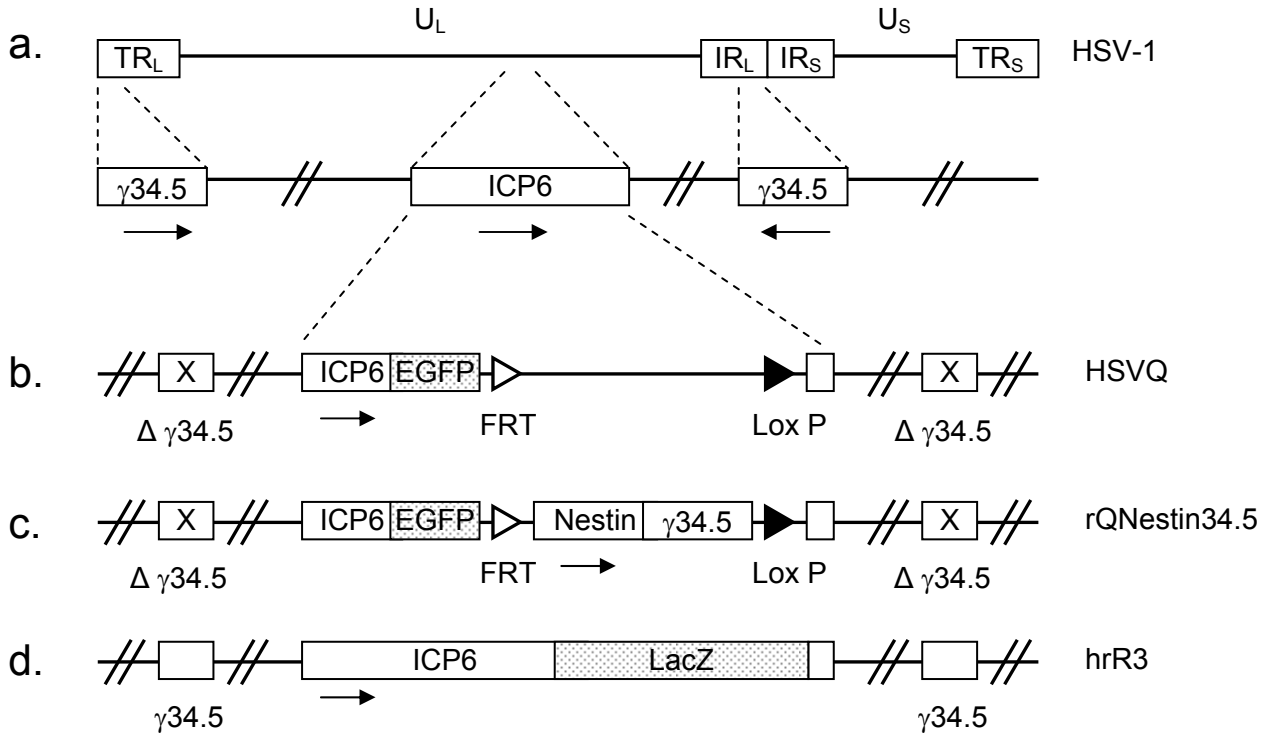

Schematic of wild type HSV-1 and the various HSV-1 derived oncolytic viruses used in this study.

a: HSV-1 genome structure showing the U_L (Unique long sequences) and U_S (Unique small sequences). Enlargements of the U_L region depict the *γ34.5* and *ICP6* domains.

b: HSVQ is an HSV-1 derived virus with deletions of both *γ34.5* genes, as well as the interruption of *ICP6* by an insertion of *EGFP*. This renders the virus unable to replicate in non-dividing cells.

c: rQNestin34.5 is an HSVQ derived virus, in which one copy of the *γ34.5* gene is reinserted into the UL39 locus under a Nestin promoter, making the virus more potent in Nestin positive glioma initiating cells.

d: Schematic of hrR3 virus, in which *γ34.5* genes have been retained but *ICP6* is interrupted by an insertion of *LacZ*.

rapidly dividing glioma cells, such as those of a brain tumor, while leaving the host's normal cells uninfected. It also allows for easy visualization of infected cells by a simple staining for *LacZ* activity [3,11,51].

HSVQ is also an HSV-1-derived OV that is deleted for both the copies of its *γ34.5* gene, which is primarily responsible for the neurovirulence of the virus. Additionally, insertion of *EGFP* within its UL39 locus results in disruption of *ICP6/RR* gene, further rendering the virus replication competent only in cycling cells [50]. The inserted *EGFP* is expressed under the control of the viral *ICP6* promoter, allowing for easy visualization of infected cells by fluorescent microscopy. rONestin34.5 is derived from HSVQ, in which one copy of the *γ34.5* gene under the governance of glioma specific Nestin promoter is reinserted into the UL39 locus. This makes the virus have more potent replication in Nestin positive glioma initiating cells [11,51].

Animal Surgery

All animal experiments were performed according to the Subcommittee on Research Animal Care of The Ohio State University guidelines. Fischer rats, aged 8 to 10 weeks, were purchased from Taconic (Taconic Farms, Germantown, NY) for *in vivo* study. After the anesthetized rats were fixed in a stereotactic apparatus, a burr hole was drilled at 2 mm lateral to the bregma, to a depth of 3 mm. Rat glioma D74/HveC cells (2×10^5 cells in 2 µl HBSS) were implanted as outlined [11]. One group of rats received an i.p. injection of CPA (Bristol-Myers Squibb, Princeton, NJ) five days after tumor implantation at a dose of 80 mg/kg of phosphate buffered saline (PBS). Seven days after tumor cell implantation, anesthetized rats were stereotactically inoculated with 1×10^7 P.F.U of rHSVQ suspended in 5 µl HBSS at the same coordinates. Animals were closely monitored for any signs of morbidity, and were euthanized

three days after infection. Tumor-bearing right hemispheres were excised and processed for RNA as described.

Athymic nude mice, aged 6 to 8 weeks, were purchased from Charles River Laboratories (Charles River Laboratories, Inc., at NCI-Frederick Animal Production Area, Frederick, Maryland) for *in vivo* study. After the anesthetized mice were fixed in a stereotactic apparatus, a burr hole was drilled at 2 mm lateral to the bregma, to a depth of 3 mm. Human glioma U87ΔEGFR cells (2 x 10^5 cells in 2 μl HBSS) were implanted as outlined [11]. Ten days after tumor cell implantation, anesthetized mice were stereotactically inoculated with 1 x 10^7 P.F.U. of rHSVQ suspended in 5 μl HBSS at the same coordinates. Animals were observed daily and were euthanized three days after infection. Tumor-bearing right hemispheres were excised and processed for RNA as described.

Immunofluorescence Staining

Brains from sacrificed animals were extracted and fixed in 4% paraformaldehyde (PFA). After being dehydrated in 30% sucrose, the brains were frozen in an isopropanol dry-ice bath. Frozen brains were then sectioned to a thickness of 10 μm by cryostat (LEICA CM3050S). The brain sections were thawed and rehydrated in PBS prior to staining. 10% normal goat serum (NGS) was used to block endogenous proteins and peroxidases by incubation at room temperature for 1 hour. Tissue sections were washed in PBS and then incubated for 1 hour at room temperature in goat α-rabbit IgG-Alexa 546, a conjugated primary antibody (1:200 dilution in PBS) (Molecular Probes, #A11034). This antibody is conjugated to a fluorescent agent, so that when it binds to the antigen of interest – in this case CYR61 – the antigen's presence can be visualized by fluorescent confocal microscopy. The brain sections were washed again in PBS and then incubated for 30 minutes at room temperature and in the dark in DAPI (1:10,000

dilution in PBS) (Sigma, #D8417). DAPI binds strongly to DNA and is thus useful for visualizing cellular density in tumor areas. DAPI fluorescence acts as a control for analyzing the antigen of interest. After another wash in PBS, the slides were fixed using Prolong™ Antifade Kit (Molecular Probes, #P7481).

RNA Preparation

Each 10 cm plate of cells *in vitro* was washed twice with 3 ml PBS. In an RNAase-free hood, 2 ml of Trizol reagent (Invitrogen, #15596-026) was added to each plate. This reagent allows the RNA to remain intact while dissolving other cell components. After 5 minutes of shaking at room temperature, the suspension was transferred to two 1.5 ml Eppendorf tubes. 200 µl chloroform was added to each tube to separate the aqueous and organic phases. The tubes were then shaken vigorously by hand for 15 seconds, rested for 3 minutes, and centrifuged at 16.3 x 1000 g for 15 mins at 4°C. After centrifugation, 3 phases were visible; the bottom organic phase contained most of the cellular proteins, the intermediate interphase contained cellular DNA, and the top aqueous phase contained cellular RNA. The RNA was precipitated from the aqueous phase by adding 1 ml isopropanol, followed by centrifugation at 16.3 x 1000 g at 4°C. The resulting RNA pellet was washed with 2 ml 75% ethanol, followed again by centrifugation at 16.3 x 1000 g for 10 minutes at 4°C. The air-dried pellet was resuspended in 25 µl of Ultrapure water.

In vivo samples were prepared by sectioning the brain after sacrificing the animal to isolate the tumor area. The tumor samples were then treated with 2 ml Trizol reagent and homogenized by syringe. The samples were then treated with 200 µl chloroform, centrifuged, and RNA was precipitated as outlined above.

Isolated RNA was cleaned using an RNeasy Mini Kit (Qiagen, #74104) according to the manufacturer's instructions. Briefly, a mixture of Cellular RNA, RLT lysis buffer, ethanol and β-mercaptoethanol was applied to an RNeasy mini spin column and centrifuged at 10,000 rpm for 15 seconds. The spin columns were washed with 350 µl Buffer RW1 and then treated with DNase I for 15 minutes at room temperature, followed by three more washes. Finally, RNA was eluted in 30-50 µl RNase-free water and was quantified.

cDNA Synthesis

cDNA was made following a standard protocol as described by SuperScript™ First-Strand Synthesis System for RT-PCR (Invitrogen, 11904-018). Briefly, 5 µg of purified RNA was incubated with 1 µl 10mM dNTP mix, 1 µl Oligo$(dT)_{12\text{-}18}$(0.5 µg/µl), and 10 µl DEPC-treated water at 65°C for 5 minutes, and then was placed on ice for 1 minute. A reaction mixture consisting of 2 µl 10x RT buffer, 4 µl 25 mM $MgCl_2$, 2 µl 0.1 M DTT, and 1 µl RNaseOUT™ Recombinant RNase Inhibitor was added to an aliquot of the RNA/primer mixtures, which were then mixed gently and centrifuged briefly. The samples were incubated for 2 minutes at 42°C. Then, 1 µl (50 units) of SuperScript™ II RT (Invitrogen, 11904-018) was added to each tube, mixed, and allowed to incubate for 50 minutes at 42°C. The reactions were terminated by incubation at 70°C for 15 minutes and were then chilled on ice briefly. Each reaction was incubated with 1 µl of RNase H, after which the tubes were incubated for 20 minutes at 37°C.

Quantitative Real-Time PCR (QRT-PCR)

Quantitative Real-Time PCR (QRT-PCR) was performed to confirm the up-regulation of CYR61 upon virus infection by analyzing the cDNA derived from infected cells. Real-time continuous detection of PCR product is facilitated by monitoring the increase in fluorescence of SYBR Green, which binds to the double stranded DNA generated during each cycle of the PCR

reaction. This fluorescence is quantified to determine relative amounts of DNA in the initial sample. Briefly, to each well of a 96-well plate, 2.5 µl of the indicated forward and reverse primers, 2.5 µl Ultrapure water, 12.5 µl SYBR Green (Applied Biosystems, #4304437), and 5 µl cDNA sample was added. The reaction plate was sealed and centrifuged for 3 minutes at 1200 rpm and QRT-PCR was performed using a 7500 real-time PCR system (Applied Biosystems, Foster, CA). Samples were amplified in triplicate. Glyceraldehyde-3-phosphate dehydrogenase (GAPDH) and β-actin were used as internal controls for all human and rat samples, respectively. Relative quantification of gene expression was calculated as a ratio of the difference in the number of cycles needed for expression of a gene in a tumor from untreated and treated rats. The formula used was 2dCt CYR61/2dCt control, where Ct is the number of cycles for saturation and dCt is the difference between the number of cycles needed for expression of a gene in a tumor from untreated rats (used as a baseline) and for expression from rats receiving treatment (tumor or tumor plus virus).

Primers for LacZ, β-actin, GAPDH, and CYR61 were designed with the Primer Express Program (Applied Biosystems) **(Table 2)**.

Agarose Gel Electrophoresis

Agarose gel electrophoresis was used to confirm the fidelity of QRT-PCR reactions. A 1.5% agarose gel was made in 1x TAE. 2 µl ethidium bromide was added to the dissolved agarose, after which the gel was poured and allowed to set. The samples were prepared by adding 2 µl orange dye to 10 µl of the QRT-PCR sample. The gel was run at 100 V.

Harvesting Cells in Culture

The conditioned medium was harvested and cleared of cellular debris by centrifugation at 4000 rpm for 10 minutes. The resulting supernatant was stored at -20°C. Cells were harvested

Table 2: Primers Used in QRT-PCR Analysis.

Primer		Primer sequence	Species
LacZ	Sense	5' – AAT GGC TTT CGC TAC CTG – 3'	E. Coli
	Antisense	5' – CCA TCG CGT GGG CGT A – 3'	
β-actin	Sense	5' – CTA CAG ATC ATG TTT GAG ACC TTC AAC – 3'	Rat
	Antisense	5' – CCA GAG GCA TAC AGG GAC AAC – 3'	
GAPDH	Sense	5' – GGA GTC AAC GGA TTT GGT CG – 3'	Human
	Antisense	5' – GGA ATC ATA TTG GAA CAT GTA AAC C – 3'	
CYR61	Sense	5' – AGA GGT GTT GAG CAT CGT GGA G – 3'	Rat
	Antisense	5' – AAC TGC GAC TGC GTT ACT GTC C – 3'	
	Sense	5' – AAT GGA GCC TCG CAT CCT ATA – 3'	Human
	Antisense	5'– TTC TTT CAC AAG GCG GCA – 3'	

Sequences of primers used in QRT-PCR analysis.

Primers for LacZ, a protein encoded by the mutant OVs, were used to evaluate viral presence in tissue samples taken from OV treated tumors in a rat glioma model. Rat β-actin primers were used to quantify actin expression in cell lysate samples, and were thus used as an internal control in evaluating CYR61 in rat glioma cell lines *in vitro* and *in vivo*. Similarly, human GAPDH was used as an internal control for samples derived from human glioma cell lines *in vitro* and *in vivo*. CYR61 was used to assess CYR61 expression in both rat and human cell lines, *in vitro* and *in vivo*, and thus primers produced in both species were used in this study.

by lysing cells in lysis buffer (8M Urea, 4% SDS, and protease inhibitor cocktail tablet [Complete Mini, #11 836 153 001]). A rubber policeman was used to scrape the cells, and the cell lysate samples were also stored at -20°C. After cell harvest, tissue culture plates were incubated with lysis buffer at 85°C for 1 hour to harvest the insoluble, plate-bound extracellular matrix (ECM). The conditioned medium and ECM were further concentrated by Trichloroacetic acid (TCA) precipitation.

TCA Precipitation

Trichloroacetic acid (TCA) is a strong acid that effectively precipitates proteins, DNA, RNA and other macromolecules from harvested samples. TCA precipitation was used to concentrate proteins from dilute CM and ECM samples, as well as to remove TCA soluble impurities. 50% ice cold TCA was added until the final TCA concentration was 15% in the conditioned medium or ECM. The samples were incubated on ice for 30 minutes, followed by centrifugation at 10,500 g for 30 minutes at 4°C. The pellets were washed twice with 1 ml of ice cold acetone and then centrifuged for 20 minutes (same as before). Air-dried pellets were rehydrated and resuspended in urea lysis buffer. Cell lysates were sonicated and then centrifuged at 12,000 rpm for 8 minutes. After protein quantification, these samples were evaluated for protein content by Western Blot analysis.

SDS Preparation of *In Vivo* Samples

After removing the brain from the sacrificed animal, the tissue sample was suspended in an equal weight of RIPA buffer (150 mM NaCl in 40 ml, 1% Nonidet P-40, 0.5% Sodium deoxycholate, 0.1% SDS, 150 mM Tris, protease inhibitor cocktail tablet [Complete Mini, #11 836 153 001]; pH = 8.0). The samples were homogenized by syringe and centrifuged (10,000 g,

10 minutes at 4°C). The supernatant was decanted to assess protein content by Western Blot analysis following protein quantification.

Protein Quantification

To quantify the protein content of each sample, an *RC DC* Protein Assay kit was used to perform a microfuge tube assay according to the manufacturer's instructions (Bio-Rad, #500-0119). Briefly, 3-5 dilutions of a protein standard were prepared from 0.2 mg/ml to 1.5 mg/ml protein, 25 µl of which was pipetted into clean microfuge tubes. The protocol was modified by adding 25 µl of *RC* Reagent I to each tube. These tubes were then vortexed and incubated at room temperature for 1 hour. The protocol was modified again when 25 µl *RC* Reagent II was added to the samples, which were then vortexed and centrifuged at 15,000 g for 3-5 minutes. The supernatant was discarded, and the precipitate was dissolved in 25.4 µl of Reagent A' (5 µl *DC* Reagent S, 250 µl *DC* Reagent A). The tubes were incubated at room temperature for 5 minutes, and vortexed briefly. To each tube was added 200 µl DC Reagent B, followed immedatiately by vortexing and incubation at room temperature for 15 minutes. The absorbances were then read at 750 nm.

Western Blot Analysis

Equal amounts of protein from the soluble supernatant was added to 6x SDS loading buffer (1 µl loading buffer : 5 µl cell sample). The prepared samples were denatured and reduced by boiling at 95°C for 4 minutes in the presence of reducing SDS dye. The samples were resolved by polyacrylamide gel electrophoresis in a Criterion precast gel (Bio-rad, #345-0009) to separate the proteins based on molecular weight. After electrophoresis, the proteins were transferred to a PVDF transfer membrane (Immobilon, #IPVH 20200) by electroblotting, in

which an electric current moves the proteins from the gel to the membrane. Transfers were completed at 220 mAmps.

Membranes were blocked in 5% non-fat milk in PBST 0.1% (block buffer) overnight at 4ºC, to inhibit non specific interactions between the membrane and the chosen antibodies. Primary antibody, which binds to the protein of interest on the membrane, was diluted in block buffer and applied to the membranes for 1 hour. The membranes were then washed three times for five minutes in PBST 0.1% to remove unbound and nonspecifically bound primary antibody. The membranes were incubated with a secondary antibody (also diluted in block buffer) that was raised against the primary and conjugated to horseradish peroxidase to facilitate detection. Because multiple secondary antibodies can bind to a single bound primary, this step results in amplification of the signal. The membranes were washed three times for 10 minutes in PBST 0.1% to remove unbound and nonspecifically bound antibodies. The membranes were developed using ECL Western Blotting Detection System (Amersham Biosciences, #RPN2132). This system contains a substrate that luminesces upon reacting with a reporter on the secondary antibody. As a result, relative amounts of protein can be determined by comparing the luminescence of the samples.

To probe for **CYR61**, pAb anti-CYR61 (Rabbit) (Novus Biologicals, #NB100-357) in a 1:750 dilution of 5% blocking milk was used for the primary antibody. The secondary antibody was Polyclonal Goat Anti-Rabbit Immunoglobulins/HRP (Dakocytomation, #P0448) in a 1:1,000 dilution of PBST 0.1%.

To probe for **β-actin**, Monoclonal Anti β-actin antibody produced in mouse (Sigma, #A1978-200) in a 1:2,000 dilution of 5% blocking milk was used for the primary antibody. The

secondary antibody was ECL Anti-Mouse IgG, horseradish peroxidase linked whole antibody (from sheep) (Amersham Biosciences, #NA931V) in a 1:20,000 dilution of PBST 0.1%.

Microvessel Density Quanitification

Following tumor implantation (Day 0) and OV infection (Day 7), the rats were monitored for signs of morbidity. Five minutes prior to euthanization, the rats were injected by tail vein with 0.25 ml of 1 mg/ml fluorescein isothiocyanate-dextran (FITC-dextran; >60 kDa) (Sigma-Aldrich, MO). FITC-dextran remains within blood vessels, thereby highlighting the animal's functional, perfused blood vessels. After removing and sectioning the brains of sacrificed animals, the entire tumor section was scanned microscopically at a low magnification (4x) to identify hotspots, or areas of high vascularization. The individual tumor microvessels that comprise these hotspots were then counted under high magnification (20x) to obtain a vessel count in a defined area. Microvessel density was defined as the average of 3 distinct hotspot vessel counts. Microvessel counting was performed in multiple tumor sections (n = 5 rats/group).

Statistical Analysis

The statistical analysis appearing in figure legends was obtained using Student's t-test and Wilcox's test. *P*-values less than 0.05 were considered significant, and data was presented as the mean +/- standard deviation.

The relative value of each QRT-PCR group was compared using a one-way ANOVA followed by a Scheffe´ post hoc test. Significance was assumed if the *P*-value was less than 0.05. Again, data was presented as the mean +/- standard deviation.

Results

Transcript Profiling Reveals Induction of CYR61 mRNA in Rat Glioma Tumors Treated with Oncolytic hrR3

Initial studies of the temporal presence of OV in rat brain tumor models revealed that the virus was cleared rapidly from tumor tissue by innate immune responses elicited upon infection [29,52-54]. Apart from host immune responses, recent studies have also underscored the significance of tumor microenvironment as a limitation to viral spread [23,24]. We believe that changes in tumor microenvironment will have a very significant impact on OV therapy.

To understand the changes in tumor environment, Dr. Kaur's laboratory has been evaluating the transcript profiling of tumors treated with OV. The laboratory has exploited CPA enhancement of OV therapy to understand the changes in gene expression tumors that occur after OV treatment in a syngeneic rat glioma model. Transient immune suppression of animals by CPA treatment prior to OV therapy results in increased viral presence in tumor tissue. The increased viral persistence enables greater tumor destruction and, thus, increases the therapeutic efficacy of the OV [28,29]. The experimental protocol is detailed in "Materials and Methods." Briefly, five days following intracerebral tumor implantation (2×10^5 D74/HveC rat glioma cells), rats were treated with an intraperitoneal injection of CPA or PBS (control), followed by an intratumoral injection of hrR3 virus on Day 7. The rats were sacrificed and brain tumors harvested at 12 and 72 hours after OV infection. RNA from these samples was isolated and converted to cDNA, which was then analyzed by gene chip assay (Affymetrix Genechip Rat Genome 230 2.0 Array) **(Figure 7a)**. Using over 31,000 probe sets, this array analyzed for more than 30,000 transcripts and over 28,000 rat genes.

Figure 7: Transcript Profiling of Rat Glioma Tumors Treated with OV and CPA Revealed a Significant Induction of CYR61.

a.

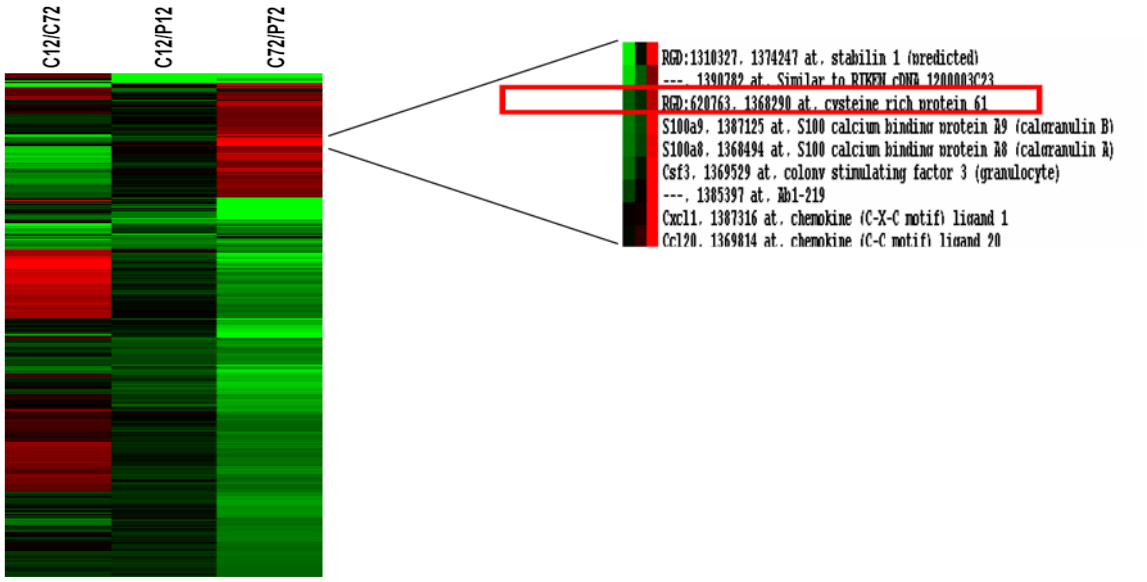

b.

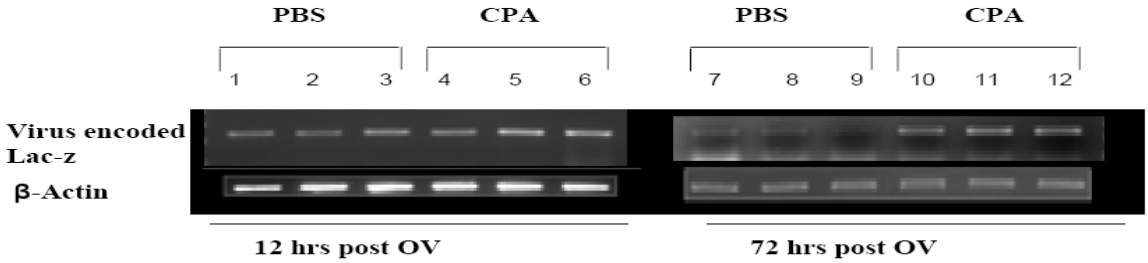

Microcluster Analysis via gene chip QRT-PCR reveals up regulation of CYR61 72 hours post infection of rat glioma tumors. Viral presence at 72 hours post infection is confirmed by agarose gel electrophoresis of virally encoded LacZ QRT-PCR product.

a: Gene chip QRT-PCR microcluster analysis of genes dysregulated by CPA pretreatment in rat brain tumors harvested 12 and 72 hours post hrR3 infection. Animals were pretreated with PBS/CPA 5 days after tumor implantation, and treated with hrR3 virus on day 7. Total RNA from tumors was harvested 12 and 72 hours after OV treatment, and changes in gene expression were evaluated by Affymatrix gene chip analysis. Upregulation is shown in red, downregulation in green, and no change in black. Note the upregulation of CYR61 mRNA in CPA treated animals at 72 hours, but not 12 hours, post infection.

b: Verification by Agarose gel electrophoresis of QRT-PCR product of OV encoded LacZ in animals treated with PBS/CPA on day 5 after tumor implantation, followed by OV infection on day 7. 12 hours post OV infection, no difference is observed between samples treated with PBS and CPA (lanes 1-3 versus 4-6). 72 hours post infection, however, rapid clearance of PBS is contrasted with sustained OV presence in CPA pretreated animals (lanes 7-9 versus 10-12). β-actin probes for actin, a protein found in most mammalian cells, and is used here as a control.

Figure 7b represents RT-PCR analysis for LacZ encoded by the OV. Note that at early time points (12 hours) post OV therapy, the presence of OV is not significantly changed in tumor tissue derived from either control PBS-treated or CPA-treated rats **(compare lanes 1-3 with 4-6)**. However, at 72 hours post infection, the rapid clearance of OV in PBS-treated animals is notable compared to the sustained presence of virus in animals pretreated with CPA **(compare lanes 7-9 with 10-12)**. This persistent viral presence in CPA-treated animals correlates with the upregulation of CYR61 seen in the microcluster analysis at 72 hours post infection.

The observation of increased CYR61 mRNA in the tumor tissue of CPA-treated rats 72 hours after OV therapy was very interesting because:

1. The induction of CYR61 mirrored the presence of virus in the tumor tissue, which indicated that CYR61 might be exploited as an interesting biomarker for OV therapy.
2. CYR61 is a secreted extracellular matrix protein known to play a very important role in tumor progression.

Confirmation of CYR61 Induction by Quantitative Real-Time PCR (QRT-PCR) Analysis

We used Quantitative RT-PCR to confirm the induction of CYR61 in rat brain tumors 72 hours post infection with OV. We formed four test treatment groups of nine animals each: control (PBS treated), CPA only, OV only, and CPA + OV. The animals were treated with PBS/CPA 5 days after tumor implantation. Two days after this treatment (Day 7 after tumor implantation), PBS/hrR3 virus was administered by direct intratumoral injection. The animals were sacrificed, and total RNA from brain tumor tissue was harvested 72 hours after infection. These samples were then analyzed by QRT-PCR with primers for CYR61 and β-actin **(Figure 8a)**. The fold-induction of CYR61 over actin in each sample was calculated.

Figure 8: QRT-PCR Results Indicate a Correlation between CYR61 Induction and OV in Rat Brain Tumors.

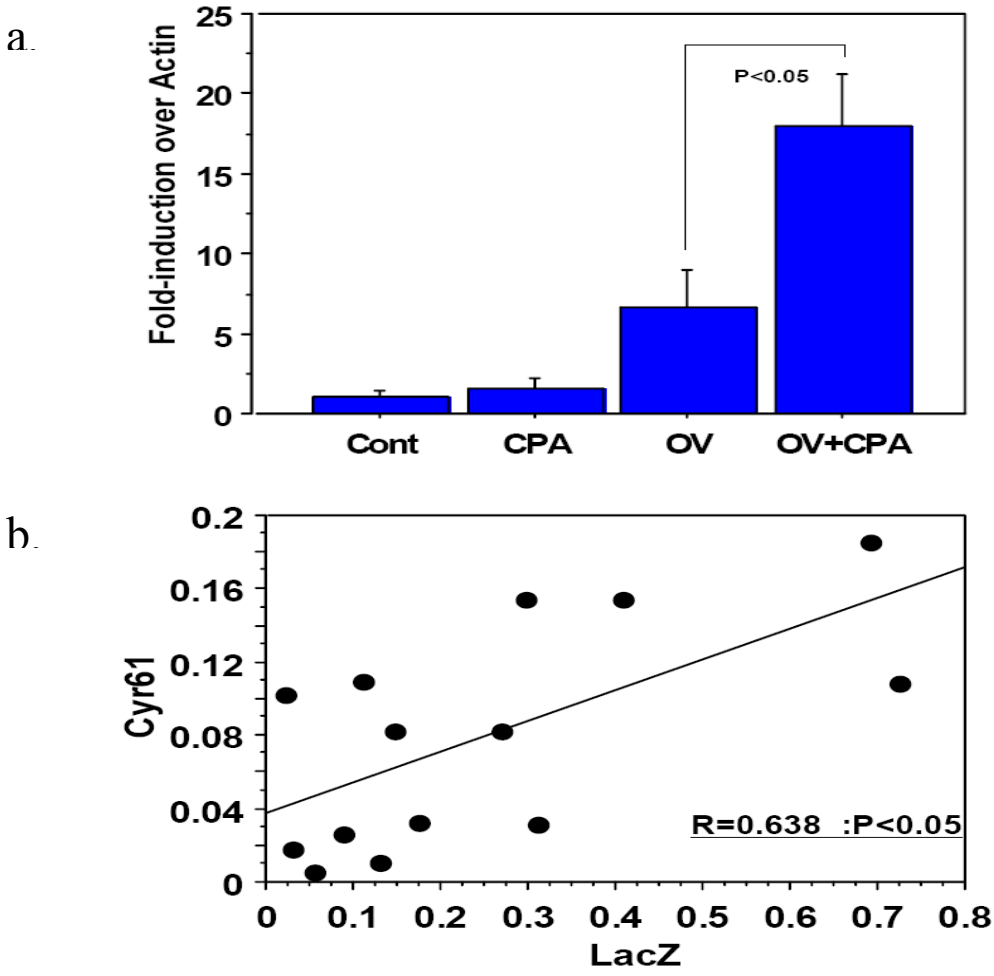

QRT-PCR and scatter plot analyses reveal a compelling correlation between viral presence and CYR61 mRNA expression at 72 hours post infection.

a: QRT-PCR for CYR61 gene expression in rat brain tumors 72 hours after PBS/OV treatment (n=9/group). After tumor implantation, animals were pretreated with PBS/OV on day 5, and PBS/OV on day 7. 72 hours after infection the animals were sacrificed. Control and CPA groups show no significant induction of CYR61, while animals treated with OV only show slight induction. Note that the significant increase in CYR61 gene expression in animals treated with both CPA and OV correlates to the previously observed prolonged viral presence in CPA pretreated animals.

b: Scatter plot analysis of the LacZ and CYR61 QRT-PCR product of the same rat glioma tumors, both with and without CPA pretreatment (n=18). The graph reveals significant positive correlation between CYR61 and virally encoded LacZ expression, indicating CYR61 induction is association with increased viral presence.

The results show mean expression of CYR61 in tumor tissue derived from all the animals in each group (n = 9/group). CYR61 expression was not significantly induced in animals that did not receive OV treatment (PBS- or CPA-treated). Tumor tissue obtained from animals treated with only OV showed slight induction of CYR61 (7.5-fold-induction over actin). This induction was significantly enhanced in tumor tissue obtained from OV-treated animals that were pretreated with CPA (17.5-fold-induction over actin; $P < 0.05$ for induction over OV-only group). Because our previous findings show that viral clearance is inhibited by CPA pretreatment, we can infer that CYR61 mRNA induction is correlated to the ongoing presence of OV in these animals.

Correlation between CYR61 Induction and hrR3 in Rat Brain Tumors

To test the significance of this perceived correlation between CYR61 expression and viral presence in tumors, we performed scatter plot analysis of virally encoded LacZ and CYR61 expression in each OV-infected tumor tissue **(Figure 8b)**. The scatter plot analysis included animals treated with and without CPA whose brain tumors were harvested 72 hours post infection (n = 18). Animals pretreated with PBS are concentrated to the left of the graph, where LacZ expression is low. These animals also exhibit low expression of CYR61. Similarly, animals pretreated with CPA consequently express high amounts of LacZ and express a large amount of CYR61. Thus, the scatter plot reveals a compelling correlation between CYR61 and virally encoded LacZ mRNA expression and gives further evidence of the association between CYR61 induction and viral presence ($R = 0.638$, $P < 0.05$).

Induction of CYR61 upon hrR3 Infection of Glioma Cells *in Vitro*

Solid tumors are very complex tissue that comprises tumor cells and normal fibroblasts as well as inflammatory cells, endothelial, and pericyte cells embedded in a complex extracellular

matrix. The CYR61 mRNA in tumor tissue could result from OV-induced infiltration into tumor tissue that expresses CYR61. However, the positive correlation observed between CYR61 expression and OV presence, irrespective of whether animals were immune suppressed with CPA pretreatment, highlighted the possibility that CYR61 may be induced directly upon OV infection of tumor tissue.

We tested this by evaluating changes in CYR61 expression in glioma cells infected with OV *in vitro*. 1×10^6 D74/HVeC rat glioma cells were plated in 10-cm dishes and infected 24 hours later with hrR3 virus (MOI = 0.05). The cell lysates were harvested at 0, 4, 8, and 24 hours post infection. Total RNA was isolated and converted to cDNA, as described in "Materials and Methods." cDNA derived from the rat glioma cells was then analyzed for CYR61 and actin expression by QRT-PCR. Samples were standardized with β-actin; our results show the fold-induction over actin expression. The results indicated a significant and early increase in CYR61 mRNA expression after OV infection **(Figure 9)**. Expression increased from 0 to 4 hours post infection, and very slightly from 4 to 8 hours. In the interval between 8 and 24 hours, however, CYR61 expression increased significantly. The HSV lytic cycle is about 12 to 16 hours, and this upsurge in CYR61 expression coincides with the viral burst. Hence, this increase at 24 hours after initial infection may represent increased infection from the second amplified round of viral progeny released after the first round of replication. This may indicate a dose-response relationship between CYR61 induction and viral infection.

Induction of CYR61 in Glioma Cells upon Infection by Three Different HSV-1-Derived OVs *in Vitro*

Next, we tested if induction of cellular CYR61 could be reproduced by infection of glioma cells with different OVs. To do this, we employed three different HSV-1-derived OVs:

Figure 9: Induction of CYR61 upon OV Infection of Glioma Cells, *in Vitro*.

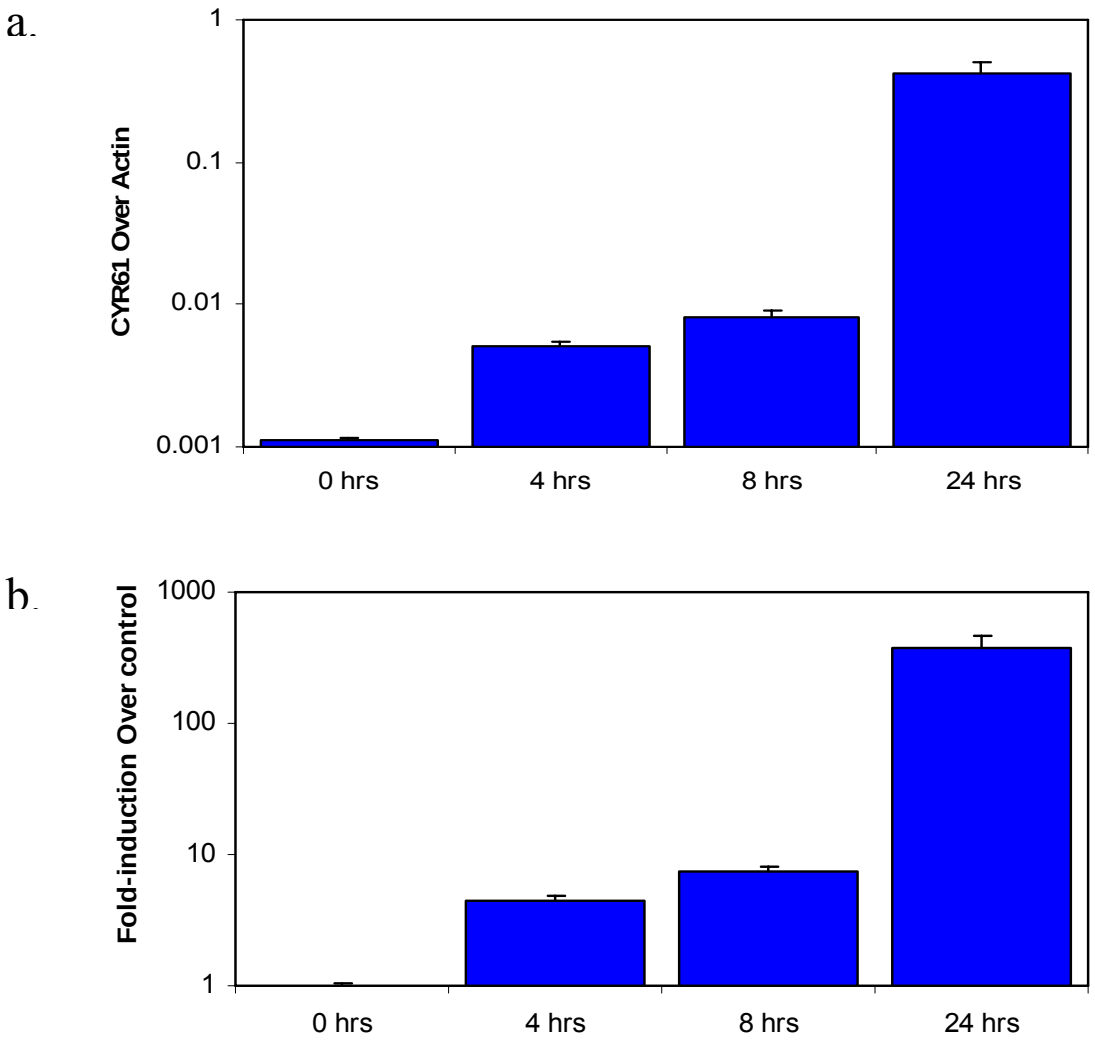

Time course QRT-PCR analysis reveals induction of Cyr61 mRNA upon OV infection of D74 rat glioma cells *in vitro*.

a: D74 cells were infected with hrR3 *in vitro*, and cell lysates were harvested 0, 4, 8, and 24 hours post infection. Following RNA isolation and cDNA synthesis, the samples were analyzed for CYR61 expression via QRT-PCR. The results were standardized by evaluating CYR61 fold-induction over actin expression in each sample. Note the increase in level of CYR61 mRNA expression at each time point. Furthermore, the magnitude of the increases in CYR61 expression correspond to the viral life cycle, thereby providing further evidence for CYR61's induction upon OV infection.

b: The same data has been normalized to uninfected cells, showing the fold-induction of CYR61 expression in infected cells.

hrR3, HSVQ, and rQNestin34.5. The structures and genetic mutations of each of these viruses are detailed in "Materials and Methods" and in **Figure 6**. 1×10^6 D74/HVeC rat glioma cells were plated in 10-cm dishes and infected 24 hours later with the indicated OV (MOI = 0.05). The cell lysates were harvested 30 hours after infection, and total RNA was isolated and converted to cDNA as described in "Materials and Methods." The cDNA was evaluated for CYR61 expression by QRT-PCR, as described. Again, the samples were standardized by calculating the fold-induction over actin expression in each RNA sample. Note the significantly increased level of CYR61 in samples infected with hrR3, HSVQ, and rQNestin34.5 in comparison to uninfected cells **(Figure 10)**. These results indicate that CYR61 is induced in response to OV infection and is not a response specific to the previously tested hrR3 virus.

Induction of CYR61 mRNA upon OV Infection in Human Glioma Cells *in Vitro*

These results indicated a rapid and significant induction of CYR61 after OV infection of rat D74/HveC glioma cells *in vitro*. Next, we evaluated if CYR61 mRNA would be similarly induced in human glioma cells after infection with HSV-1-derived OV. We tested this in human glioma cell lines (LN229, U343, U87, and U87ΔEGFR) and in primary tumor cells from patient biopsy. These cells are curated by the Dardinger Laboratory at The Ohio State University and were obtained from Dr. Otsuki. The tumor characteristics of these patient-derived tumor cells are described in "Materials and Methods" and in **Table 1**. On Day 0, 1×10^5 of the indicated cells were plated in a 10-cm dish. The cells were treated with PBS or rQNestin34.5 virus on Day 1 (MOI = 1). Total cellular RNA was isolated 24 hours after infection, converted to cDNA, and was analyzed by QRT-PCR as described in "Materials and Methods." GAPDH served as an internal control, resulting in data that reflects CYR61 expression as a fold-induction over GAPDH expression in each sample. The data were normalized to the levels of CYR61 in a

Figure 10: Induction of CYR61 in Glioma Cells upon Infection by Various HSV-1-Derived OVs, *in Vitro*.

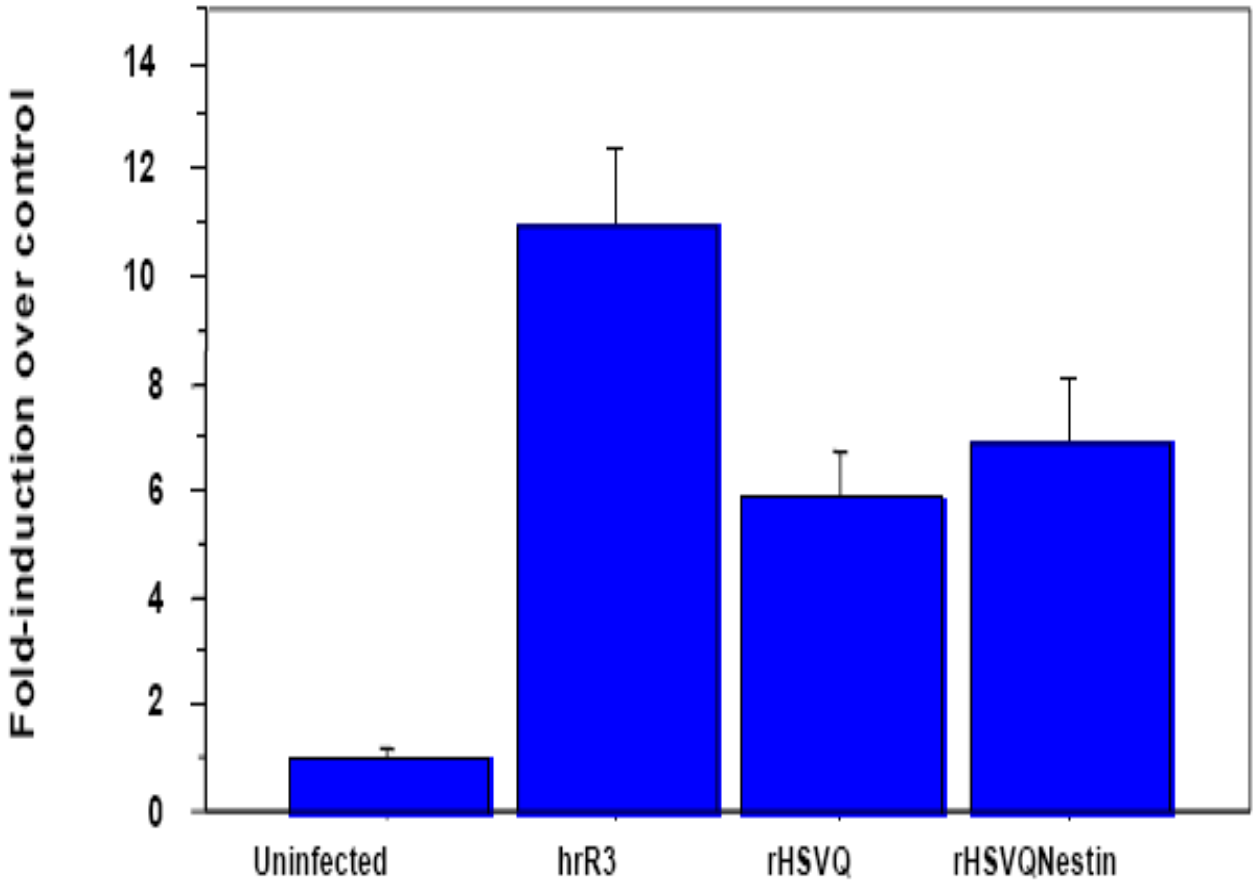

The upregulation of CYR61 mRNA 30 hours post infection of D74 rat glioma cells in vitro using three different HSV-1 derived OVs.

D74 rat glioma cells were infected with the hrR3, HSVQ, or rQNestin34.5 *in vitro*. Cell lysates were harvested 30 hours post infection. Isolated RNA was converted to cDNA, after which the samples were analyzed by QRT-PCR. The results were standardized by evaluating CYR61 fold-induction over actin expression in each sample. Note the significantly increased level of CYR61 mRNA expression in each of the three OVs when compared to the uninfected sample.

normal brain sample obtained from an epileptic lobectomy. The fold-induction of infected cells over uninfected cells for each cell line indicated a significant increase in CYR61 mRNA expression in all the cell lines tested **(Table 3)**. The increased levels of CYR61 mRNA expression upon OV infection in each tumor cell line provide evidence that CYR61 induction is a direct result of OV infection and occurs in a wide variety of human glioma cells.

Induction of CYR61 Protein Expression upon OV Infection of Human Glioma *in Vitro*

To evaluate if induction of CYR61 mRNA also translated into increased levels of protein after HSV infection, we evaluated changes in levels of CYR61 protein after infection with OV *in vitro*. U343 human glioma cells were infected with either hrR3 (MOI = 0.1) or PBS. The cells were harvested 16 hours after infection, and the amount of CYR61 in cell lysate and ECM was evaluated by Western blot analysis, as detailed in "Materials and Methods." The results indicate an increase in both the secreted full length and proteolytically processed form of CYR61 in the ECM of OV-infected cells **(Figure 11a)**. Plasmin cleavage of CYR61 has previously been shown to liberate CYR61 protein from the ECM, and thereby plays a role in many of CYR61's pathophysiologic processes involved in tumor growth and angiogenesis [55]. Our findings also show an increase in CYR61 protein in the cell lysate after OV infection. The membrane was also probed for actin as an internal control, which reveals that CYR61 expression is also significantly upregulated in the cell lysate **(Figure 11b)**.

Induction of CYR61 Protein Expression upon OV Infection of Human Glioma *in Vivo*

Next, we investigated if CYR61 protein induction is observed *in vivo*. U87ΔEGFR human glioma cells were implanted in athymic nude mice by intracerebral injection. The animals were injected intratumorally with either OV or PBS on Day 7 following implantation,

Table 3: Induction of CYR61 mRNA upon OV Infection in Several Human Glioma Cells, *in Vitro*.

Glioma cells	Uninfected (CYR61 /GAPDH)	Infected (CYR61 /GAPDH)	Fold Induced (Infected /Uninfected)	P Value
PATIENT BIOPSY DERIVED CELLS				
OG02	45.7	218.8	4.8	0.00650
# 9.0	8.5	30.2	3.5	0.00700
OG06	12.1	34.7	2.9	0.00180
# 8.0	12.8	19.9	1.6	0.00310
OG09	4.7	12.5	2.7	0.00030
GLIOMA CELL LINES				
LN229	3.3	30.7	9.3	0.0005
U87	1.1	3.8	3.6	<0.0001
U343	4.0	10.0	2.5	0.0090
U87ΔEGFR	1.3	2.8	2.2	0.0150

Induction of CYR61 upon OV infection is confirmed in multiple human glioma and patient derived tumor cell lines.

The listed human glioma cell lines and patient derived tumor cells were each treated with PBS or rQNestin 34.5 for 24 hours (MOI = 1). The cells were the harvested and analyzed by QRT-PCR. The samples were analyzed for the amount of CYR61 relative to the amount of GAPDH (an internal control) expressed by the cells. The results were normalized to the levels in a normal brain. Note the induction of CYR61 mRNA expression upon OV infection in each tumor cell line.

Figure 11: Induction of CYR61 Protein *in Vitro* after Infection of Human Glioma Cells.

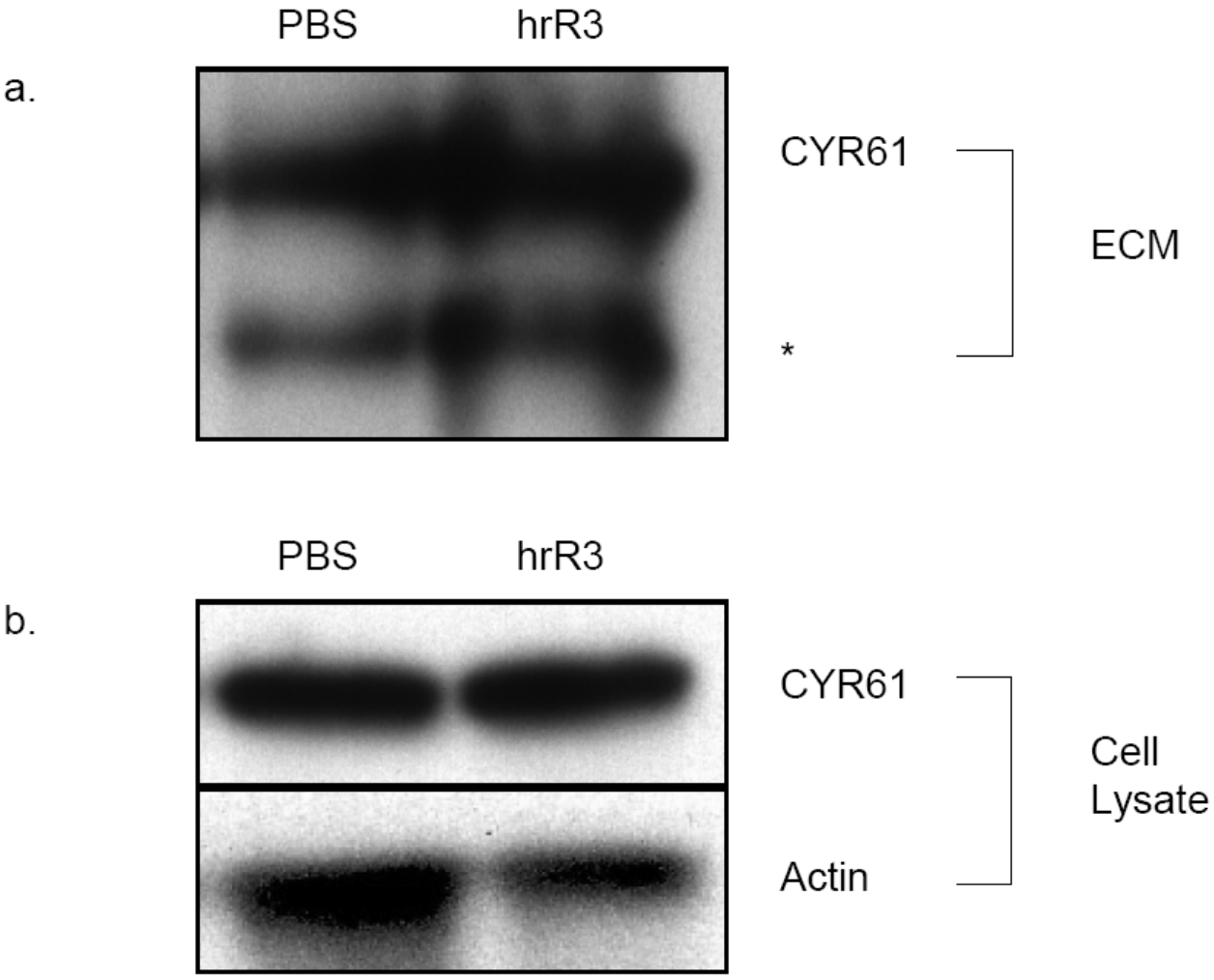

Western blot analysis reveals induction of CYR61 protein *in vitro* upon infection of human glioma U343 cells.

a: U343 human glioma cells were infected with either hrR3 or PBS. After 16 hours of infection, the ECM was harvested and evaluated for CYR61 expression by western blot analysis. Note the substantial increase in CYR61 protein secreted into the ECM in cells treated with HSV-1-derived OV over those treated with PBS. ∗Indicates a proteolytic fragment of CYR61 [56].

b: From the same samples, cell lysates were also harvested that display an increase CYR61 expression relative to actin expression in cells treated with hrR3.

and tumors were harvested at 24 and 48 hours after infection. These tissue samples were evaluated for CYR61 expression by Western blot analysis and were normalized to actin expression. The results clearly indicate an increase in CYR61 protein expression in infected cells when compared to the uninfected sample **(Figure 12)**.

We also assessed *in vivo* CYR61 protein induction by immunofluorescence staining. U87ΔEGFR human glioma tumor cells were implanted to form intracerebral tumors in athymic nude mice, as described. Seven days after tumor implantation, the tumors were treated with PBS/rQNestin34.5 by direct intracerebral injection. The mice were euthanized and the tumors harvested at 72 hours post infection. The tissue samples were then stained for CYR61 and DAPI expression **(Figure 13)**. DAPI, which stains for cellular nuclei, allows visualization of cell density. Highly dense DAPI fluorescence represents areas of high cellular density, or areas of tumor. A comparison of the tumor edge as depicted by stainings for DAPI and for CYR61 reveals that very little CYR61 is expressed in the PBS-treated control group. In contrast, staining for CYR61 in the OV group reveals significant induction of CYR61 protein expression. Furthermore, this protein expression is localized to the tumor region; the tumor edge, as depicted by DAPI staining, matches that of the boundary of CYR61 expression for the tumor treated with OV. These results indicate that CYR61 protein expression is also induced upon OV infection in the athymic nude mouse model *in vivo*.

Induction of Angiogenic Inducer CYR61 upon OV Treatment Leads to Increased Microvessel Density of the Residual Disease

CYR61 is known to be a potent angiogenic inducer [34,38,47,56]. Furthermore, elevated levels of CYR61 are sustained after blood vessel formation in endothelial cells, suggesting that the protein also functions in vessel maintenance. Studies have also shown that CYR61 plays a

Figure 12: Induction of CYR61 Protein *in Vivo* after OV Infection of Human Glioma Cells.

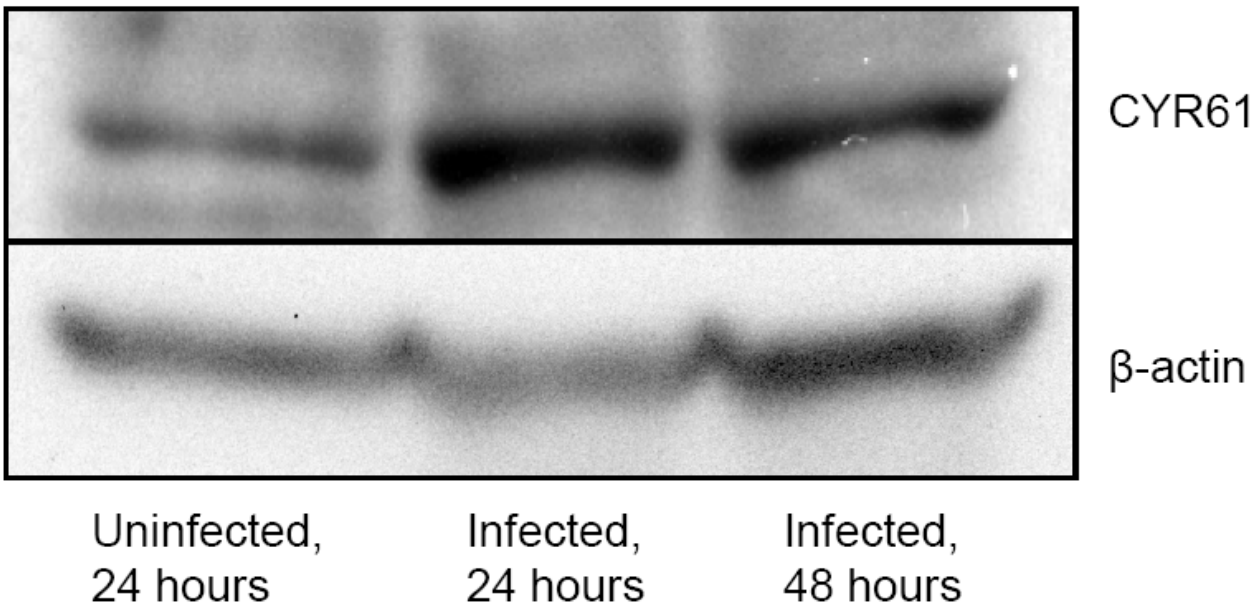

Western blot analysis reveals induction of CYR61 protein *in vivo* upon infection of human glioma U87ΔEGFR cells.

U87ΔEGFR human glioma cells were implanted in athymic nude mice by intracerebral injection. On Day 7, either OV or PBS was administered intratumorally. The animals were sacrificed and brain tissues harvested 24 and 48 hours after infection. Using western blot analysis, the samples were evaluated for CYR61 expression (45 kDa) relative to actin expression (44 kDa). The results show a considerable increase in CYR61 protein expression in OV treated tumors in comparison to uninfected tumors *in vivo*.

Figure 13: Induction of CYR61 Protein Expression upon OV Infection of Intracerebral Tumors in Athymic Nude Mice.

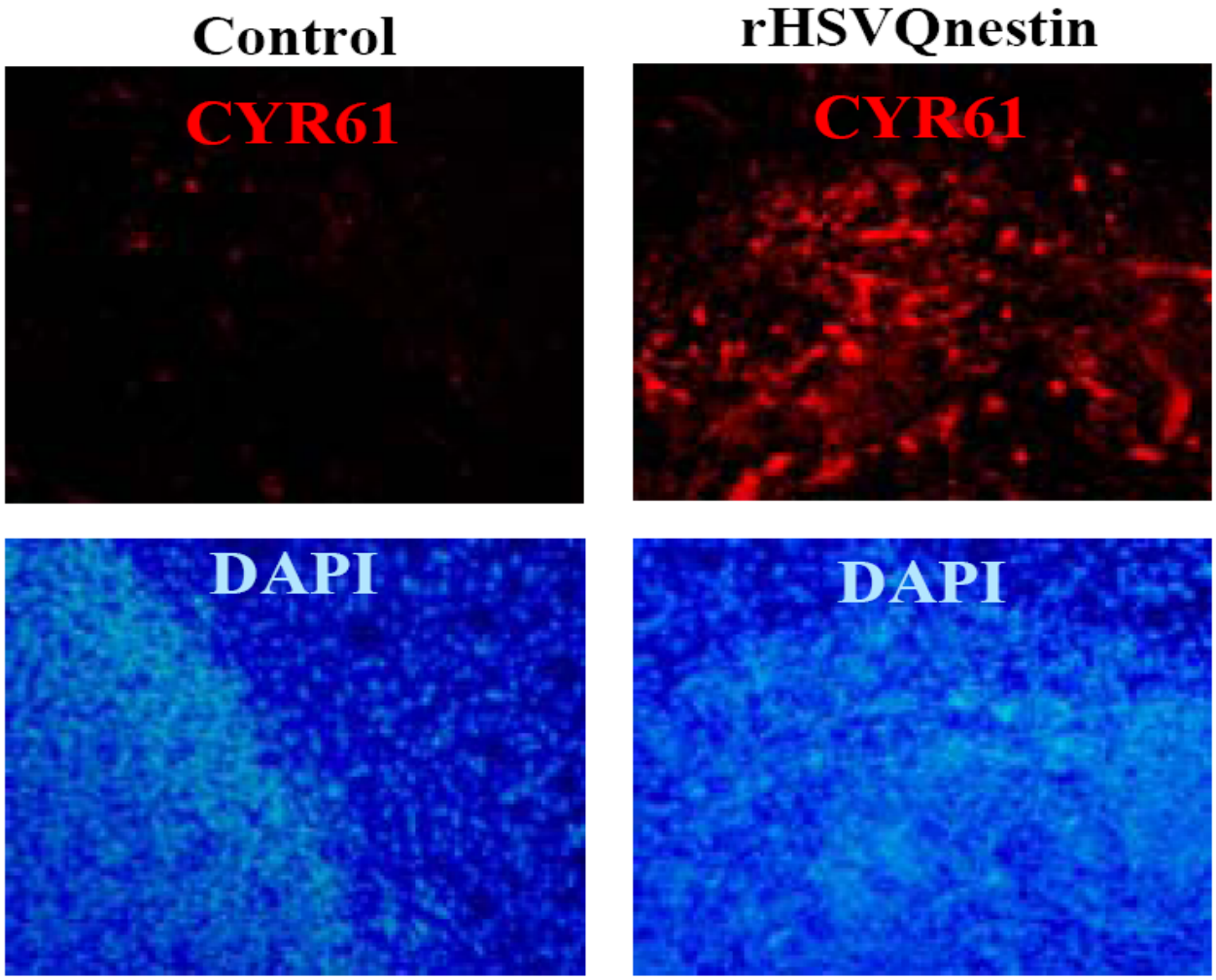

Immunofluorescence staining for CYR61 protein expression reveals induction of CYR61 protein upon OV infection of intracerebral tumors in athymic nude mice.

Intracerebral brain tumors (U87ΔEGFR cells) were implanted in athymic nude mice. These tumors were treated with either PBS (control group) or rQNestin34.5 (OV group) on day 7. 72 hours post infection, the mice were sacrificed and the harvested tumors were analyzed for CYR61 and DAPI protein expression by immunofluorescence staining. DAPI depicts cellular density; the edges of tumor regions are visible in these stainings. The CYR61 staining corresponding to these frames reveals a significant induction of CYR61 protein expression upon OV infection. Furthermore, the CYR61 protein is localized to the tumor region in the tumor treated with OV, thus giving further evidence of CYR61's association with viral presence.

significant role in neovascularization *in vivo* [34]. We therefore hypothesized that an increase in secreted levels of CYR61 protein in a tumor's extracellular matrix after oncolysis would lead to increased angiogenesis of the residual disease. This could lead to an aggressive recurrence of the tumor and may contribute to the reduced efficacy of OV observed in clinical trials.

We tested this by comparing the microvessel density of untreated and OV-treated size-matched tumors in the rat glioma model. PBS-treated (mean survival, Day 14) and hrR3-treated (mean survival, Day 21) animals were sacrificed upon showing signs of morbidity. Five minutes prior to euthanization, the rats received tail-vein injections of dextran conjugated to FITC (> 60kDa). This compound was used to stain perfused or circulating blood vessels in the tumor region. A comparison of size-matched tumors derived from control PBS-injected animals (original disease) and tumors from animals treated with OV (recurrent disease) showed an increase in microvessel density **(Figure 14a)**. Quantification of the number of blood vessels per field of view revealed a significant induction of angiogenesis in recurrent tumor after OV treatment when compared to untreated PBS control tumors **(Figure 14b, $P < 0.05$)**. The highly angiogenic nature of the residual disease may contribute toward reducing the efficacy of OV therapy. This result has implications towards designing future clinical trials in conjunction with anti-angiogenic treatment.

Figure 14: Induction of CYR61, an Angiogenic Factor, upon OV Treatment Leads to Increased Microvessel Density of the Residual Disease.

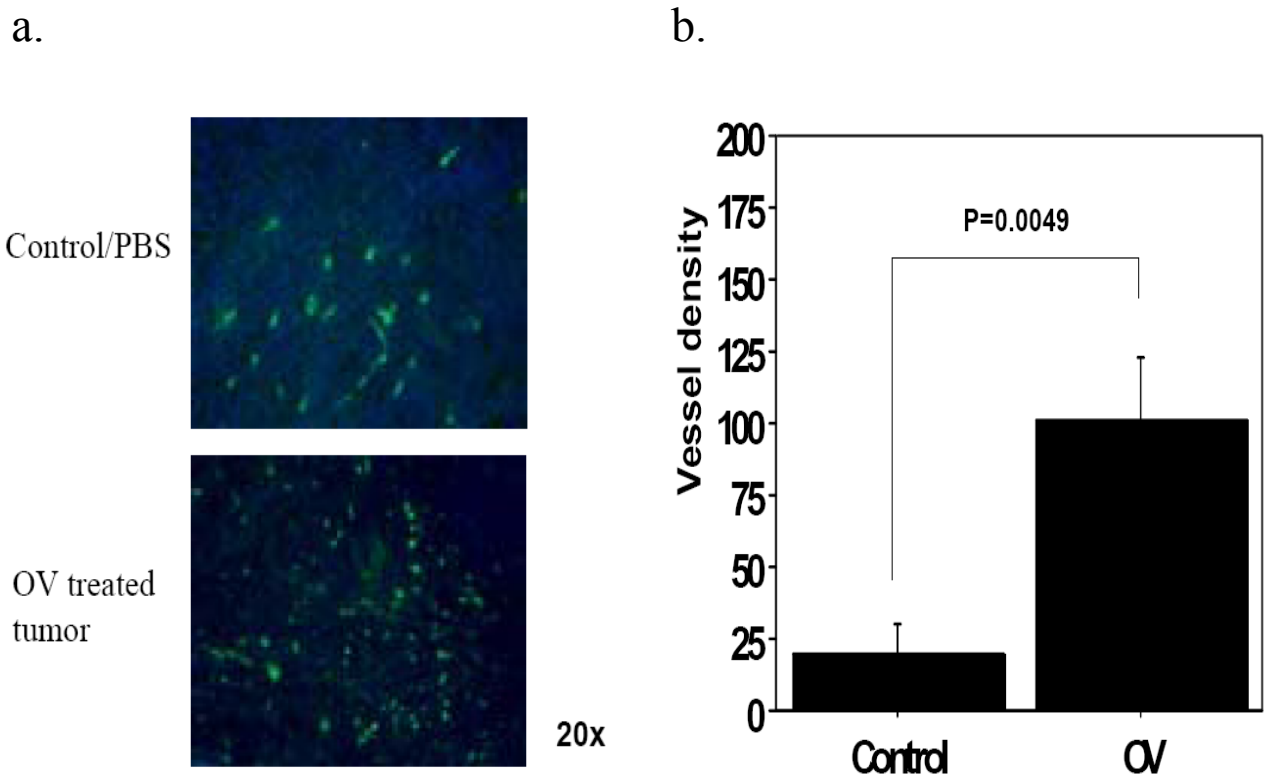

Increased microvessel density of residual disease after OV treatment is the result of induction of CYR61, an angiogenic inducer, upon OV treatment.

a: PBS/OV treated animals were sacrificed when they showed signs of morbidity (Day 14 for PBS-treated, Day 21 for OV-treated). 5 minutes prior to euthanization, the rats were tail vein injected with dextran conjugated to FITC (>60kDa) to stain perfused blood vessels in the tumor region. A significant increase in microvessel density of residual disease after OV treatment is clearly visible when compared to the PBS treated tumor.

b: Microvessel density was quantified by counting the number of vessels per view field. The angiogenic activity induced by CYR61 expression in the residual tumor is evident when compared to the untreated tumor sample ($P<0.05$). The induction of neovascularization by CYR61 protein may lead to an aggressive recurrence of the residual tumor post OV therapy.

Discussions and Conclusions

OV-mediated tumor destruction is an exciting experimental therapy that is currently being tested in clinical trials. These trials have revealed the incredible safety of OV treatment, wherein none to minimal signs of toxicity could be attributed directly to the virus [3,57]. Nevertheless, the high expectations of this therapeutic modality remain unmet. Changes in the tumor microenvironment induced by OV therapy can significantly impact the treatment's effectiveness by altering the growth and spread of solid tumors [58,59]. Given the complicated interactions between cancerous cells and their microenvironment, we hypothesized that OV induced changes in the tumor environment would dictate the efficacy of this therapeutic modality.

Here, we describe for the first time the induction of CYR61 upon OV infection of glioma cells. CYR61 mRNA induction has been validated in multiple human glioma cell lines, as well as in patient derived tumor cells. Furthermore, mRNA induction was observed upon infection with three different HSV-1-derived OVs. Our study also confirms the induction of CYR61 protein expression following OV treatment both *in vitro* and *in vivo*. The consistent induction of CYR61 mRNA and protein expression upon OV infection indicates that this secreted protein can serve as a biomarker for OV activity; an elevation in CYR61 levels will accurately reflect ongoing viral infection, replication, and propagation.

In addition, future studies investigating the mechanism of CYR61 induction could lead to the generation of imaging vectors that drive the expression of marker proteins under the governance of this OV inducible promoter. These vectors can then be used to reflect OV activity, thereby allowing viral activity to be monitored in a non-invasive manner. These studies would allow individual patient responses observed in clinical trials to be correlated to OV

activity in each patient by monitoring and evaluating changes in CYR61 levels in the patient's tumor following OV treatment. In addition, these studies may further clarify the interplay between the host's innate viral clearing and adaptive anti-tumor immune responses and their effects upon OV therapy's efficacy.

Ongoing studies in the laboratory are exploring the effect of CYR61 on subsequent rounds of viral infection/replication and/or propagation in tumor tissue. The effect of CYR61 on viral therapy is as yet unclear; the protein may function either to stimulate or inhibit subsequent viral treatments. Thus, future studies in the laboratory will be aimed at investigating the potential of using CYR61 levels in tumors as prognostic markers to predict patients who would benefit from OV therapy.

Given the magnitude of tumor vasculature's effect upon the tumor microenvironment, it is also probable that changes in tumor vasculature will greatly affect the outcome of OV therapy [60]. Our studies show the effect of CYR61 protein in changing the biology of the residual disease by increasing angiogenesis after OV therapy. These results reveal the importance of treating the tumor microenvironment alongside the cancerous cell to yield synergistic enhancement of therapy.

This study lays down a rationale for the treatment of tumors with OV in conjunction with anti-angiogenic agents to target both cancerous cells and tumor microenvironment. Future studies will identify the feasibility of using CYR61 as a potential biomarker for OV activity *in vivo*.

References

1. Xie, D. et al. Levels of expression of CYR61 and CTGF are prognostic for tumor progression and survival of individuals with gliomas. *Clin Cancer Res* **10**, 2072-81 (2004).
2. Brat, D.J., Castellano-Sanchez, A., Kaur, B. & Van Meir, E.G. Genetic and biologic progression in astrocytomas and their relation to angiogenic dysregulation. *Adv Anat Pathol* **9**, 24-36 (2002).
3. Cutter, J.L., Kurozumi, K., Chiocca, E.A. & Kaur, B. Gene therapeutics: the future of brain tumor therapy? *Expert Rev Anticancer Ther* **6**, 1053-64 (2006).
4. Kaur, B. & Chiocca, E.A. Oncolytic viruses: extreme treatment for an extreme disease. *Future Microbiology* **1**, 351-353 (2006).
5. Aguilar-Cordova, E. Vectorology recapitulates virology--will it capitulate oncology? *Nat Biotechnol* **21**, 756-7 (2003).
6. Sinkovics, J.G. & Horvath, J.C. Newcastle disease virus (NDV): brief history of its oncolytic strains. *J Clin Virol* **16**, 1-15 (2000).
7. Ni, S. et al. Evaluation of biodistribution and safety of adenovirus vectors containing group B fibers after intravenous injection into baboons. *Human Gene Therapy* **16**, 664-677 (2005).
8. Chiocca, E.A. et al. A phase I open-label, dose-escalation, multi-institutional trial of injection with an E1B-Attenuated adenovirus, ONYX-015, into the peritumoral region of recurrent malignant gliomas, in the adjuvant setting. *Mol Ther* **10**, 958-66 (2004).
9. Lawler, S.E., Peruzzi, P.P. & Chiocca, E.A. Genetic strategies for brain tumor therapy. *Cancer Gene Ther* **13**, 225-33 (2006).
10. Varghese, S. & Rabkin, S.D. Oncolytic herpes simplex virus vectors for cancer virotherapy. *Cancer Gene Ther* **9**, 967-78 (2002).
11. Kambara, H., Okano, H., Chiocca, E.A. & Saeki, Y. An oncolytic HSV-1 mutant expressing ICP34.5 under control of a nestin promoter increases survival of animals even when symptomatic from a brain tumor. *Cancer Res* **65**, 2832-9 (2005).
12. Boviatsis, E.J. et al. Gene transfer into experimental brain tumors mediated by adenovirus, herpes simplex virus, and retrovirus vectors. *Hum Gene Ther* **5**, 183-91 (1994).
13. Boviatsis, E.J. et al. Antitumor activity and reporter gene transfer into rat brain neoplasms inoculated with herpes simplex virus vectors defective in thymidine kinase or ribonucleotide reductase. *Gene Ther* **1**, 323-31 (1994).
14. Ichikawa, T. & Chiocca, E.A. Comparative analyses of transgene delivery and expression in tumors inoculated with a replication-conditional or -defective viral vector. *Cancer Res* **61**, 5336-9 (2001).
15. Hedley, S.J. et al. An adenovirus vector with a chimeric fiber incorporating stabilized single chain antibody achieves targeted gene delivery. *Gene Ther* (2005).
16. Borovjagin, A.V. et al. Complex mosaicism is a novel approach to infectivity enhancement of adenovirus type 5-based vectors. *Cancer Gene Ther* **12**, 475-86 (2005).
17. Nakano, K. et al. Herpes simplex virus targeting to the EGF receptor by a gD-specific soluble bridging molecule. *Mol Ther* **11**, 617-26 (2005).

18. Hallak, L.K., Merchan, J.R., Storgard, C.M., Loftus, J.C. & Russell, S.J. Targeted measles virus vector displaying echistatin infects endothelial cells via alpha(v)beta3 and leads to tumor regression. *Cancer Res* **65**, 5292-300 (2005).
19. Biglari, A. et al. Effects of ectopic decorin in modulating intracranial glioma progression in vivo, in a rat syngeneic model. *Cancer Gene Ther* **11**, 721-32 (2004).
20. Mahendra, G. et al. Antiangiogenic cancer gene therapy by adeno-associated virus 2-mediated stable expression of the soluble FMS-like tyrosine kinase-1 receptor. *Cancer Gene Ther* **12**, 26-34 (2005).
21. Kikuchi, E. et al. Inhibition of orthotopic human bladder tumor growth by lentiviral gene transfer of endostatin. *Clin Cancer Res* **10**, 1835-42 (2004).
22. Finger C., e.a. Replicating retroviral vectors mediating continuous production and secretion of therapeutic gene products from cancer cells. *Cancer Gene Ther* **12**, 464-74 (2005).
23. Kim, J.H. et al. Relaxin expression from tumor-targeting adenoviruses and its intratumoral spread, apoptosis induction, and efficacy. *J Natl Cancer Inst* **98**, 1482-93 (2006).
24. McKee, T.D. et al. Degradation of fibrillar collagen in a human melanoma xenograft improves the efficacy of an oncolytic herpes simplex virus vector. *Cancer Res* **66**, 2509-13 (2006).
25. McCormick, F. Future prospects for oncolytic therapy. *Oncogene* **24**, 7817-9 (2005).
26. Abordo-Adesida, E. et al. Stability of lentiviral vector-mediated transgene expression in the brain in the presence of systemic antivector immune responses. *Hum Gene Ther* **16**, 741-51 (2005).
27. Balachandran, S., Thomas, E. & Barber, G.N. A FADD-dependent innate immune mechanism in mammalian cells. *Nature* **432**, 401-5 (2004).
28. Fulci, G. et al. Cyclophosphamide enhances glioma virotherapy by inhibiting innate immune responses. *Proc Natl Acad Sci U S A* **103**, 12873-8 (2006).
29. Wakimoto, H., Fulci, G., Tyminski, E. & Chiocca, E.A. Altered expression of antiviral cytokine mRNAs associated with cyclophosphamide's enhancement of viral oncolysis. *Gene Ther* **11**, 214-23 (2004).
30. Andreansky, S. et al. Treatment of intracranial gliomas in immunocompetent mice using herpes simplex viruses that express murine interleukins. *Gene Ther* **5**, 121-30 (1998).
31. Bennett, J.J. et al. Interleukin 12 secretion enhances antitumor efficacy of oncolytic herpes simplex viral therapy for colorectal cancer. *Ann Surg* **233**, 819-26 (2001).
32. Todo, T., Martuza, R.L., Dallman, M.J. & Rabkin, S.D. In situ expression of soluble B7-1 in the context of oncolytic herpes simplex virus induces potent antitumor immunity. *Cancer Res* **61**, 153-61 (2001).
33. Kim, S.M. et al. Coxsackievirus B3 infection induces cyr61 activation via JNK to mediate cell death. *J Virol* **78**, 13479-88 (2004).
34. Latinkic, B.V. et al. Promoter function of the angiogenic inducer Cyr61gene in transgenic mice: tissue specificity, inducibility during wound healing, and role of the serum response element. *Endocrinology* **142**, 2549-57 (2001).
35. Xie, D. et al. Cyr61 is overexpressed in gliomas and involved in integrin-linked kinase-mediated Akt and beta-catenin-TCF/Lef signaling pathways. *Cancer Res* **64**, 1987-96 (2004).

36. Smith, S.J., Fairclough, L., Latinkic, B.V., Sparrow, D.B. & Mohun, T.J. Xenopus laevis transgenesis by sperm nuclear injection. *Nat Protoc* **1**, 2195-203 (2006).
37. Yang, G.P. & Lau, L.F. Cyr61, product of a growth factor-inducible immediate early gene, is associated with the extracellular matrix and the cell surface. *Cell Growth Differ* **2**, 351-7 (1991).
38. Kireeva, M.L., Mo, F.E., Yang, G.P. & Lau, L.F. Cyr61, a product of a growth factor-inducible immediate-early gene, promotes cell proliferation, migration, and adhesion. *Mol Cell Biol* **16**, 1326-34 (1996).
39. Chaqour, B. & Goppelt-Struebe, M. Mechanical regulation of the Cyr61/CCN1 and CTGF/CCN2 proteins. *Febs J* **273**, 3639-49 (2006).
40. Chen, C.C., Mo, F.E. & Lau, L.F. The angiogenic factor Cyr61 activates a genetic program for wound healing in human skin fibroblasts. *J Biol Chem* **276**, 47329-37 (2001).
41. Mo, F.E. et al. CYR61 (CCN1) is essential for placental development and vascular integrity. *Mol Cell Biol* **22**, 8709-20 (2002).
42. Chaqour, B. et al. Cyr61 and CTGF are molecular markers of bladder wall remodeling after outlet obstruction. *Am J Physiol Endocrinol Metab* **283**, E765-74 (2002).
43. Chen, N., Chen, C.C. & Lau, L.F. Adhesion of human skin fibroblasts to Cyr61 is mediated through integrin alpha 6beta 1 and cell surface heparan sulfate proteoglycans. *J Biol Chem* **275**, 24953-61 (2000).
44. Grzeszkiewicz, T.M., Kirschling, D.J., Chen, N. & Lau, L.F. CYR61 stimulates human skin fibroblast migration through Integrin alpha vbeta 5 and enhances mitogenesis through integrin alpha vbeta 3, independent of its carboxyl-terminal domain. *J Biol Chem* **276**, 21943-50 (2001).
45. Kim, K.H. et al. Expression of angiogenic factor Cyr61 during neuronal cell death via the activation of c-Jun N-terminal kinase and serum response factor. *J Biol Chem* **278**, 13847-54 (2003).
46. Babic, A.M., Chen, C.C. & Lau, L.F. Fisp12/mouse connective tissue growth factor mediates endothelial cell adhesion and migration through integrin alphavbeta3, promotes endothelial cell survival, and induces angiogenesis in vivo. *Mol Cell Biol* **19**, 2958-66 (1999).
47. Babic, A.M., Kireeva, M.L., Kolesnikova, T.V. & Lau, L.F. CYR61, a product of a growth factor-inducible immediate early gene, promotes angiogenesis and tumor growth. *Proc Natl Acad Sci U S A* **95**, 6355-60 (1998).
48. Kolesnikova, T.V. & Lau, L.F. Human CYR61-mediated enhancement of bFGF-induced DNA synthesis in human umbilical vein endothelial cells. *Oncogene* **16**, 747-54 (1998).
49. Menendez, J.A., Mehmi, I., Griggs, D.W. & Lupu, R. The angiogenic factor CYR61 in breast cancer: molecular pathology and therapeutic perspectives. *Endocr Relat Cancer* **10**, 141-52 (2003).
50. Terada, K., Wakimoto, H., Tyminski, E., Chiocca, E.A. & Saeki, Y. Development of a rapid method to generate multiple oncolytic HSV vectors and their in vivo evaluation using syngeneic mouse tumor models. *Gene Ther* **13**, 705-14 (2006).
51. Chung, R.Y., Saeki, Y. & Chiocca, E.A. B-myb promoter retargeting of herpes simplex virus gamma34.5 gene-mediated virulence toward tumor and cycling cells. *J Virol* **73**, 7556-64 (1999).

52. Ikeda, K. et al. Oncolytic virus therapy of multiple tumors in the brain requires suppression of innate and elicited antiviral responses. *Nat Med* **5**, 881-7 (1999).
53. Wakimoto, H. et al. The complement response against an oncolytic virus is species-specific in its activation pathways. *Mol Ther* **5**, 275-82 (2002).
54. Wakimoto, H., Johnson, P.R., Knipe, D.M. & Chiocca, E.A. Effects of innate immunity on herpes simplex virus and its ability to kill tumor cells. *Gene Ther* **10**, 983-90 (2003).
55. Pendurthi, U.R., Tran, T.T., Post, M. & Rao, L.V. Proteolysis of CCN1 by plasmin: functional implications. *Cancer Res* **65**, 9705-11 (2005).
56. Kireeva, M.L. et al. Cyr61 and Fisp12 are both ECM-associated signaling molecules: activities, metabolism, and localization during development. Exp Cell Res 233, 63-77 (1997).
57. Aghi, M. & Martuza, R.L. Oncolytic viral therapies - the clinical experience. Oncogene 24, 7802-16 (2005).
58. de Visser, K.E., Eichten, A. & Coussens, L.M. Paradoxical roles of the immune system during cancer development. Nat Rev Cancer 6, 24-37 (2006).
59. Norton, L. & Massague, J. Is cancer a disease of self-seeding? Nat Med 12, 875-8 (2006).
60. Folkman, J. Role of angiogenesis in tumor growth and metastasis. Semin Oncol 29, 15-8 (2002).